Retrieval of Glyoxal during MAD-CAT Campaign in Mainz, Germany and IESE-NUST, Islamabad, Pakistan

By

Syeda Ifraw Naved

(NUST201362286MSCEE65213F)

A thesis submitted in partial fulfillment of the requirements for the degree of

Master of Science

In

Environmental Sciences

Institute of Environmental Sciences and Engineering (IESE)

School of Civil and Environmental Engineering (SCEE)

National University of Sciences and Technology (NUST)

Islamabad, Pakistan (2016)

This work is dedicated to my Dad and Aapi Jan

for their endless support and encouragement to bring the best out of me

and to my uncle Syed Akhtar Naz

for giving me the spirit to acquire knowledge

ACKNOWLEDGEMENTS

All praise to Allah Almighty for giving us the blessing of Wisdom.

This dissertation would not have been possible without the guidance and the help of several individuals who, in one way or another, contributed in the preparation and completion of this study.

First and foremost, I would like to express my gratitude to my supervisor ***Dr. Muhammad Fahim Khokhar*** *for the comments, remarks, engagement and positive criticism through the learning process of this master thesis.*

Furthermore, many thanks also go to ***Dr. Muhammad Zeeshan Ali Khan*** *and* ***Dr. Imran Shahid*** *(IST) who had always been very considerate and supportive in my research work.*

I am grateful to ***MAD-CAT*** *team for providing me with the data and a chance to publish my work.*

I am grateful to the staff of ***IESE, NUST*** *as they were very helpful and supportive.*

I am grateful to all members of CCARGO for being cooperative and helpful and special thanks to ***Mr. Junaid Khayam Butt*** *and* ***Mr. Zain Abbas****.*

Special thanks to ***Mr. Areej Khan*** *(CASEAN-NUST) for providing me metrological data.*

I would also like to extend my thanks to all of my friends, well-wishers and loved ones who gave me support, without whose support and understanding it would have taken a much longer time to finish this work.

Special thanks to my parents and my siblings for their consistent encouragement and endless support.

Syeda Ifraw Naveed

LIST OF ABBRIVEATIONS

CHOCHO	Glyoxal
MAD-CAT	Multi Axis DOAS-Comparison Campaign for Aerosols and Trace gases
IESE-NUST	Institute of Environmental Sciences and Engineering - National University of Sciences and Technology
MAX-DOAS	Multi Axis Differential Optical Absorption Spectroscopy
DOAS	Differential Optical Absorption Spectroscopy
DSCDs	Differential Slant Column Densities
VCDs	Vertical Column Densities
VOC	Volatile Organic Compound
SOA	Secondary Organic Aerosols
HCHO	Formaldehyde

LIST OF TABLES

Chapter 2

Chapter 3

LIST OF FIGURS

Chapter 2

Chapter 4

Table of Contents

ABSTRACT

Glyoxal being the tiniest α-dicarbonyl forms during VOC oxidation reactions. It has residence time of few hours determined by photolysis and hydroxyl radical reactions during day time. In the presence of NO_x, glyoxal photolysis results in the formation of secondary organic pollutants along with the tropospheric ozone. This is a kind of pioneer study for glyoxal retrieval in Pakistan. It presents a comparison of glyoxal retrieval from mini MAX-DOAS measurements at two different monitoring sites in Pakistan and Germany. First data set was obtained during MAD-CAT (Multi Axis DOAS-Comparison Campaign for Aerosols and Trace gases) campaign held from 18 June–13 July, 2013 in Mainz, Germany. Second data set was generated from ground based MAX-DOAS observations at IESE-NUST (Institute of Environmental Sciences and Engineering - National University of Sciences and Technology), Islamabad, Pakistan. Glyoxal differential slant column densities (DSCDs) were retrieved using DOAS (differential optical absorption spectroscopy) technique. And by using geometric air mass factor approach, tropospheric vertical column densities (VCDs) were derived from measured DSCDs. Firstly, retrieved glyoxal was compared for the month of June and July over both measurement sites in respective years. Covariant of solar irradiation, ambient air temperature and relative humidity were investigated. A significant correlation ($r > 0.8$) was observed for actinic flux and glyoxal diurnal variabilities at both study sites. A quantitative difference in glyoxal VCDs observed was mainly due to difference in actinic flux and vegetation profiles of both monitoring sites. Seasonal cycle of glyoxal was investigated for data set of IESE from October-2014 to September 2015. It exhibited good correlation with metrological parameters (solar radiation, ambient temperature and relative humidity).

CHAPTER 1

INTRODUCTION

1.1. Background

Earth's surface is accumulated by reactive organic compounds, and are released during a variety of processes occurring by Volatile Organic Compounds (VOCs) emissions. VOCs exist in air in very large amount and their reactivity greatly affects the atmospheric chemistry. VOCs acts as the predecessor of ozone and further they provide fuel for tropospheric ozone formation (Houweling *et al.,* 1998; Poisson *et al.,* 2001), this also determines the tropospheric capacity of VOCs to get reduced (Monks, 2005). They also play crucial role in regulating the formation of second order pollutants (Kanakidou *et al.,* 2005; Kostas & Kanakidou, 2003; Kostas & Kanakidou, 2007; Kostas *et al.,* 2005; Volkamer *et al.,* 2006) and influence the CCN formation (cloud condensation nuclei) (Roberts *et al.,* 2002; Yu, 2000).

VOCs chemistry also contributes in direct and indirect climate change impacts (Ramanathan & Crutzen, 2003), which in turn affects human health (Pope III & Dockery, 2006). Therefore, it's necessary to explore VOCs sources and sinks and their oxidation phenomenon.

Human activities result into emission of chemical compounds which get accumulated into troposphere. Photochemical smog produced hinders the opportunities for better living style because of highly degraded air qualities (Finlayson-Pitts & Pitts, 1999), causing threat to health of living beings (Molina & Molina, 2002), agricultural yield (Gregg *et al.,* 2003) and local climate (Ramanathan *et al.,* 2001).

1.2. Glyoxal and Air Chemistry

The performance of conventional VOC oxidation indicators such as ozone, and cumulative effect of ozone with nitrogen dioxide (NO_2) is known as O_x and methyl vinyl ketone (MVK). Principally vehicular exhaust influences this situation (Finlayson-Pitts & Pitts, 2000), also affecting the atmospheric distribution of these species. Particularly, glyoxal (CHOCHO) is produced during aromatic hydrocarbon oxidation by OH radical in the presence of NOx. Glyoxal is also known as important ring cleavage

specie in atmospheric oxidation reactions. It has also been recognized as main product of several reactions of ozone and OH radicals with VOCs and alkenes particularly those one which possess unsaturated oxygen compounds, such as acrolein, acetylene and glycolaldehyde. In urban environment, glyoxal measurements have been described with mixing ratios which range from 100 parts per trillion to a few parts per billion.

Secondary gaseous products such as organic aerosols and ozone are produced as a result of photochemical degradation of VOCs, predominantly in the presence of nitrogen oxides. Both of these products are vital contributors to air pollution causing severe health impacts. Main intermediate products produced in VOCs oxidation are formaldehyde and glyoxal.

Glyoxal being the tiniest α-dicarbonyl, having mutagenic properties (Kielhorn *et al.,* 2004), forms during VOC oxidation reactions (Calvert *et al.,* 2002; Calvert *et al.,* 2000; Volkamer *et al.,* 2001). Further, emissions from tailpipe have reported slight amounts of glyoxal (Grosjean *et al.,* 2001; Kean *et al.,* 2001). Its residence time is determined by photolysis and hydroxyl radical reactions during day time (Atkinson, 2000).

1.3. Absorption Cross-section of Glyoxal

Absorption spectrum exhibited by glyoxal lie within two major spectrum band ranges; a broad range ultra violet band lying between 220 - 350 nm and a strong structured band between 350 - 480 nm. Among these the later band contains two further band systems including one tremendously weaker having its 0 - 0 band at 520.8 nm and another comparatively stronger possessing its 0 - 0 band at 454.9 nm. Glyoxal concentrations have been measured in urban air, using DOAS (differential optical absorption spectroscopy) technique, with the sharp peak observed at 455 nm (Volkamer *et al.,* 2005).

1.4. Sources and Sinks of Glyoxal

Biogenic emissions contribute about 55% of global glyoxal concentration, anthropogenic 27% while 18% is caused by pyrogenic emissions. Photolysis (51%) is considered as major glyoxal sink, followed by secondary organic aerosol (SOA) formation (22%), oxidation of OH radical (18%) and wet and dry deposition (8%).

Important process in removal of glyoxal from atmosphere is photolysis during daytime, while hydroxyl radicals also contribute to a minor extent. Atmospheric residence time is described to be only a few hours (Fu *et al.,* 2008).

Globally glyoxal concentrations are reported to be 56 Tg annually with the lifetime of about 2.5 h which is agreed with literature studies such as 45 Tg annually with 2.9 h lifetime (Finlayson-Pitts & Pitts, 2000) and 56 Tg annually with 3 h lifetime (Myriokefalitakis *et al.,* 2008). The annual global burden of glyoxal is assessed as 15.8 Gg annually (Fu *et al.,* 2008). Another study carried out at global scale, estimations are found to be low with a difference of 20% and are mainly due to SOA sinks which are not defined (Myriokefalitakis *et al.,* 2008). Total pyrogenic emissions increased by fire emissions contribute about 60% in global glyoxal concentrations, while remaining is subsidized by secondary productions, such as acetylene oxidation, aromatics, glycoaldehyde and ethylene with contribution percentages of 24%, 5%, 4% and 7% respectively.

1.5. Pakistan and Air Pollution Issues

Among the most popular issues, air pollution is predominant, especially in the major cities of Pakistan due to rapid urbanization and vehicular exhausts. This causes several health impacts such as eye infections, reduced lung functions, skin irritations and transmission of infectious diseases. It is of great concern as the retarded lung function due to air pollution can result into lung cancer. During last few years, alarming increase in Asthmatic patients has also been observed due to outdoor air pollution. And studies prove that consistent intake of polluted air makes the diseases more complex (Ahmed, 2014).

Urban air pollution causes 80,000 hospital cases annually. In year 2005 outdoor air pollution alone caused more than 22,600 deaths in adults. Approximately 8,000 chronic bronchitis cases, and nearly 5 million respiratory infections cases in children with age under 5 are reported (Ahmed, 2014).

Pak-EPA (Pakistan Environmental Protection Agency) has conducted a number of studies to explore the root causes and pollutant concentrations in different regions of Pakistan. Which indicates that concentrations of various pollutants are above Pak-NEQS. No relevant study is found on atmospheric glyoxal over South Asia especially

in Pakistan. This study will provide a baseline for the atmospheric glyoxal because it plays vital role in atmospheric chemistry as source, intermediate and as a sink specie.

1.6. Present Study

It's a comparative study, conducted for the retrieval of glyoxal, at Mainz, Germany and Islamabad, Pakistan. Data for Mainz was collected in a campaign named, MAD-CAT and for Islamabad at ARL-IESE-NUST (Atmospheric Research Lab, Institute of Environmental Sciences and Engineering, National University of Sciences and Technology). Two different data sets were run in QDOAS software to obtain DSCDs (Diffraction Slant Column Densities) of glyoxal.

1.6.1. Importance of the Study/Research

Glyoxal is considered as one of the major and most prevailing dicarbonyls existing in the atmosphere. Mostly, high concentrations of aromatic and living species suggest that glyoxal distributions in atmosphere could be a great contributor to SOA. Further, it has been detected as a compound which produce higher glyoxal yields, referring to air hydration and polymerization (Jang & Kamens, 2001).

Health impact of glyoxal on animals has been reported by many researchers but no research has been conducted on humans. Mainly water and food possessing glyoxal concentrations are the contributing routes to human population, whereas air also plays a major role as reported in literature that almost 20 m^3 air contain about 4 µg glyoxal/m^3 Borrego *et al.*, 2000).

So for better understanding of atmospheric chemistry and air quality, it is necessary to have estimates about the actual concentration of glyoxal. The proposed methodology has been supported by many scientists and gives direct measurement with accurate result. This study can help us in following perspectives;

- Contribution in International database
- Baseline for future research in Pakistan
- Establishing a relationship between glyoxal, and anthropogenic activities

1.3.2. Objectives of the Study

1. To retrieve and compare the atmospheric glyoxal over Islamabad, Pakistan and Mainz, Germany
2. To identify the possible sources of glyoxal emissions

CHAPTER 2

LITEATURE REVIEW

2.1. Evolution of Planet Earth's Atmosphere

Atmosphere of any planet is defined as a layer of gases surrounding the planet and other material bodies of adequate masses that are detained in place by the gravitational force of the planet. The modern atmospheric state and composition is the result of evolutionary processes starting 4.5 billion years ago. Resilient volcanic eruptions caused the outgassing of water vapor and carbon dioxide that initially formed a gaseous layer around the planet. Afterwards on cooling, these water vapors formed seas and oceans. Different photochemical reactions resulted in accumulation of carbon dioxide and oxides of nitrogen. This accumulated carbon dioxide was then used by the micro-organisms in the oceans to form oxygen. Lately in Early Proterozoic era oxygen started building up in the atmosphere and ozone layer was formed (about 2.4 billion years ago) to support the appearance of first multicellular cellular life on the planet. Present atmospheric composition is given in Table. 2.1.

Table 2.1: Main atmospheric constituents, their chemical symbols and their concentrations in atmosphere (Mole Percent) (Wayne, 2000)

CONSTITUENT	CHEMICAL SYMBOL	MOLE PERCENT
Nitrogen	N_2	78.084
Oxygen	O_2	20.947
Argon	Ar	0.934
Carbon Dioxide	CO_2	0.035
Neon	Ne	0.00182
Helium	He	0.00052
Methane	CH_4	0.00017
Krypton	Kr	0.00011
Hydrogen	H_2	0.00005
Nitrous Oxide	N_2O	0.00003
Xenon	Xe	0.00001
Ozone	O_3	trace to 0.00080

2.2. Air Pollution

Depending upon the nature and its role in atmospheric chemistry, every pollutant has a fate that lies somewhere in the cycle of "emission - chemical transformation - transport - deposition", this process is schematically described in Figure 2.1. It shows the atmospheric phases of natural and anthropogenic emissions as how they are transformed chemically in presence of day light (and in absence of light as well) and at the end the left overs are deposited either through the process of wet deposition or dry deposition. Sources of these pollutants mainly lie near the ground surface but after being emitted they are chemically transported and distorted vertically and horizontally by wind currents. The ability of any pollutant to affect our health or materials in any way lies in its composition and life time. In this context short lived pollutants principally have local impacts, for example triggering atmospheric pollution issues in industrialized and urban regions, while pollutants with longer life time are transported to the larger distances and altitudes, causing global impacts.

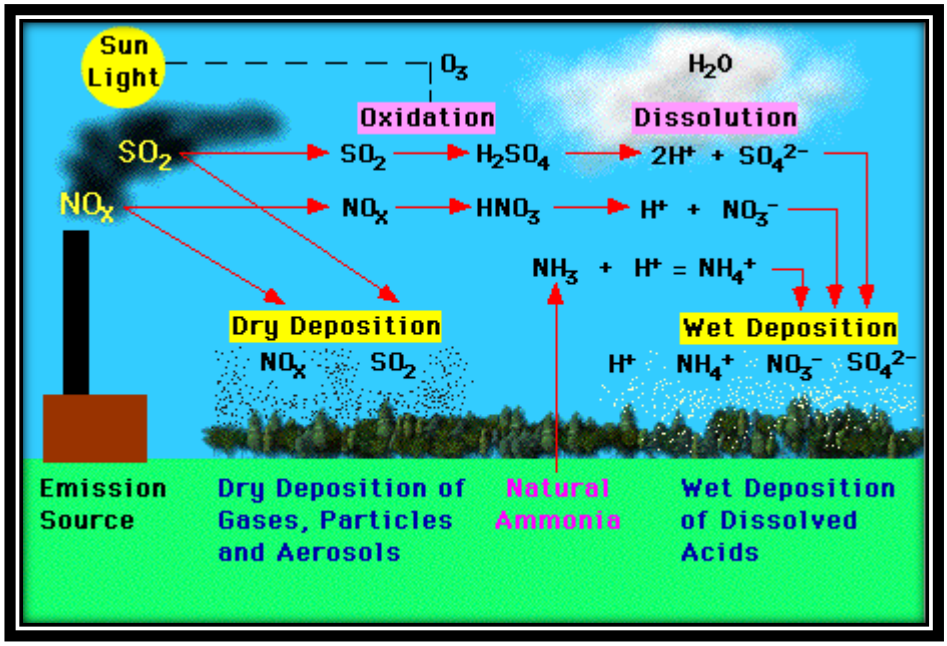

Figure 2.1: Emissions, state transformation, transportation and final deposition processes linked to the atmospheric chemistry. These progressions connect the atmosphere with supplementary mechanisms of the planetary system, including marine and terrestrial flora and fauna.

Pollutants are generally in the form of solid particles (i.e., aerosols), chemicals or fumes. Their sources can be anthropogenic as well as natural for instance volcanic emissions, biodegradation and gaseous emissions from plants accounts for natural volatile organic emissions. But we are more concerned about anthropogenic sources as

we may manage to control them. For instance, CO_2, CO, SO_2, NOx, and VOCs emissions from fossil fuel combustion (including gas, oil and coal) at domestic and commercial scale. Pollutants are either primary or secondary, depending upon the pathways of their formation. Primary pollutants are emitted directly into the air, for example exhaust from an industry or a car while secondary pollutants are produced as a result of chemical reactions among primary pollutants, for example ozone formation in troposphere (BLOEMEN, 1995).

2.3. Atmospheric Boundaries

Even though air seems as a well-mixed composite that forms our atmosphere, but physically it is not as uniform as it seems to be. It has number of layers, separated by boundaries, depending upon the varying temperature and pressure with altitude. These include;

i. Troposphere
ii. Stratosphere
iii. Mesosphere
iv. Thermosphere
    i. Ionosphere
    ii. Exosphere

2.3.1. Troposphere

Troposphere, being the lowest layer of the atmosphere, remains in contact with the ground. This layer contains the most precious gas oxygen, which we breathe in. Its thickness ranges from 0-16 km (8km at poles while 16km across equator). Troposphere contains almost 75% mass of the total atmosphere and is therefore the denser layer of atmosphere. Nitrogen and oxygen being the main components of atmosphere accounts for 78% and 21% respectively, while the left over 1% accounts for other trace gases. All the weather phenomena we experience on ground do mostly happens in this layer. In troposphere as we move above the ground surface, temperature generally falls, but in some cases it increases due to trapped air called, temperature inversion. This phenomenon is responsible for photochemical smog formation, a notorious episode of climate change.

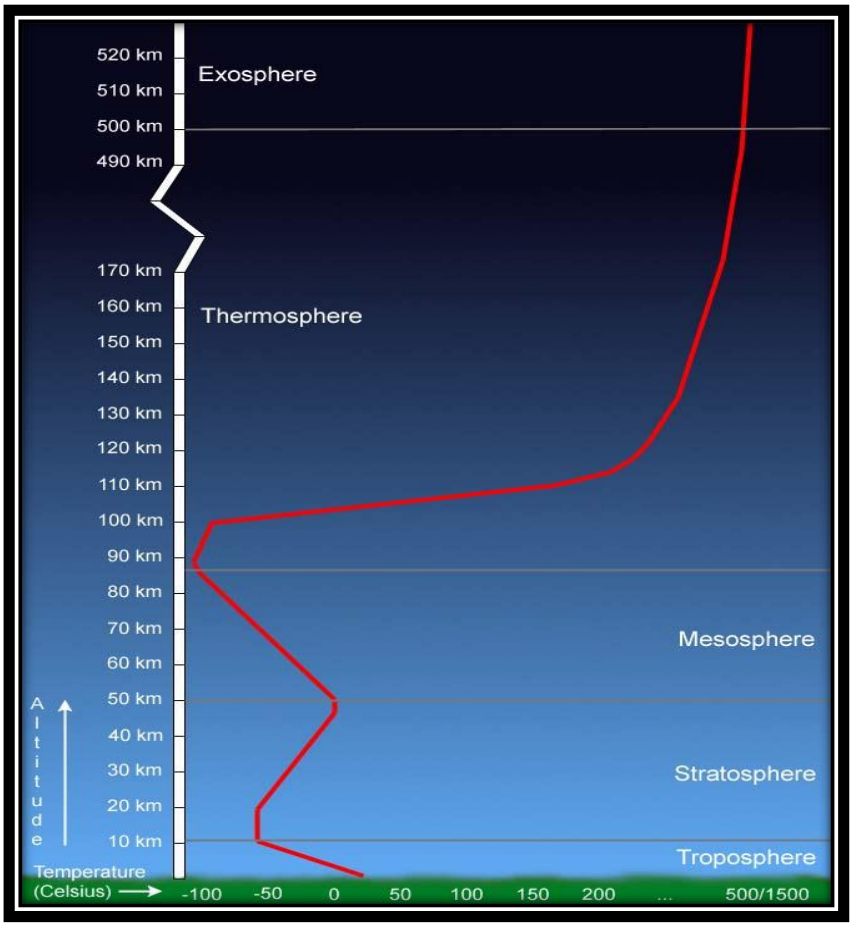

Figure 2.2: Layers of atmosphere with respect to temperature (°C), height (altitude in km) and chemical composition

2.3.2. Stratosphere

Stratosphere is the layer of atmosphere above the troposphere, separated by a boundary layer called tropopause. It is the layer that contains the most precious gift of nature, the ozone layer, which acts as a filter and traps the UV radiations coming from the Sun. This phenomenon is the reason behind the increasing temperature profile with height. Its thickness is about 12-15 km from the ground but its lower boundary has variable height at poles and equator. It is almost free of clouds and other weather forms and exhibits strong and steady horizontal wind patterns. And this property provides an advantage for long distance flights.

2.3.3. Mesosphere

Mesosphere is the layer present in 50-80 km region of atmosphere, separated from stratosphere by a boundary called, stratopause. In this layer temperature profile tends to fall with the increasing altitude (falls about -100°C). It is the coldest layer of the atmosphere, even more colder than the lowest recorded temperature at Antarctica.

This much cold causes water vapor to freeze into ice clouds, which are visible when Sun tends to 4-16 degrees down to the horizon, these clouds are called Noctilucent Clouds. That blue layer of the sky, we see is color of the mesosphere. Meteors when enter in the Earth's atmosphere got burn in this layer and seen as shooting stars from the ground.

2.3.4. Thermosphere

Thermosphere is the outer most layer of atmosphere. It is separated from mesosphere by a boundary layer called, mesopause and lies from 80-640 km in the atmosphere. Temperature of this layer rises with the altitude reaching up to 1000°C, caused by the absorption of Sun's energy by the molecules present their in.

2.3.4.1. Ionosphere

Ionosphere is the sphere present in the thermosphere layer; it is also called as lower part of thermosphere. It extends from 80-550 km in thermosphere. It contains highly ionized air, resulting from the breaking of molecule and atoms into ions due to strong solar radiations. Ionosphere is the region of atmosphere where the aurorae phenomenon occurs.

2.3.4.2. Exosphere

Exosphere exists beyond the ionosphere, starting from 550 km and extending up to 10,000 km, where atmosphere gradually merges into space. It is also called outer thermosphere, where the prime components present are helium and hydrogen. Satellites orbit our Earth in this region.

2.4. Climate Change and Global Warming

Climate change is the name of statistical changes in weather distribution patterns, when the changes last for extended time period (i.e., decades to centuries). Climate theory of Earth is constructed on the hypothesis that a balance is maintained between the amounts of energy that it absorbs in the form of UV/visible light coming from sun and the amount of heat it radiates back to the space in the form of infrared radiation. Variables responsible for change in energy balance and affecting the average temperature of the globe are called forcings since they force the temperature to rise or fall. This includes variations in sun's brightness cycles, particulate matters and aerosols

devising from volcanic eruptions, oceans, anthropogenic sources and changes in amount of heat trapping greenhouse gases (GHGs) in the atmosphere. GHGs include CO_2, CO, NOx, CH_4, O_3, CFCs and HCFCs. Among all forcings, CO_2 is playing a key role in global warming being the only variable that changes significantly by amount. CO_2 concentrations are increasing continually, reaching up to 400 ppm today, since the last recorded as 280 ppm in 1750 whereas, according to IPCC CO_2 range of natural emissions are 180 to 300 ppm. Recent oceanic studies states that, Earth's capability to sequester CO_2 naturally is decreasing, and presently the nature is sequestering almost half of the anthropogenic CO_2 being produced.

2.4.1. Trace Gases and its Effect on Global Warming

Human activities have caused a prominent increase in emission concentrations of trace gases in atmosphere that has triggered the global surface temperature to rise. Variations in natural climate are concealing this continual increase in temperature, but this effect could be doubled or quadrupled, if the trace gas emissions continued, with the present rate, for next 65 years. Climate effects caused by trace gases depend upon the interactions between radiations, atmospheric chemistry and dynamics. These chemical species include CFCs, HCFCs, CH_4, tropospheric O_3, N_2O, and stratospheric H_2O.Trace gases are driving temperature increase by direct and indirect effects in troposphere as well as in stratosphere. CFCs and HCFCs are indirectly affecting the global temperature balance by destroying stratospheric O_3 and allowing the UV radiations to enter in the troposphere. CH_4, NO_x, and CO are the driver of tropospheric O_3 production that has radiative properties in this layer. Tropospheric H_2O can trouble the tropospheric chemistry and promotes the CH_4 and O_3 production. Collectively it can be stated that indirect effects of trace gases can be as important as direct ones (Ramanathan *et al.*, 1987).

2.4.2. Photochemical Smog/Tropospheric Ozone

Smog is a form of air pollution episode; it is formed when fossil fuel emissions combine with fog. Burning of fossil fuels results in variety of pollutant emissions in the troposphere. Among the emitted pollutants, hydrocarbons and nitric oxide (NO) are most notorious. After the significant accumulation of these pollutants, a chain of reactions occurs in the presence of sunlight, which converts NO to NO_2. This NO_2 has brown color and at significantly high levels, it forms major constituent of urban haze.

And further this NO_2 breaks apart in the presence of sunlight and produces oxygen atoms which results in tropospheric O_3 formation. And this mixture of O_3 and oxides of nitrogen mixed in fog is called photochemical smog (Akimoto, 2016).

2.5. Glyoxal

Carbonyl compounds are subsets of highly reactive VOCs that significantly contributes in the formation of secondary organic aerosols (SOA) (Jang *et al.,* 2002; Finlayson-Pitts & Pitts, 2000). Carbonyls are directly released during incomplete burning of fossil fuel and biomass, or formed during photochemical oxidation of VOCs (Possanazini *et al.,* 2007). Some of the carbonyls like acetaldehyde and formaldehyde are found to have toxic and carcinogenic nature (Partridge *et al.,* 1987). Glyoxal, one of the smallest a-dicarbonyl, was found as an important precursor for SOA formation through heterogeneous and homogenous reactions (Fuv2008; Liggio *et al.,* 2005). It is among the most predominant dicarbonyls in contaminated ambient airs with 45 Tg/yr as global source (Fu *et al.,* 2008). Glyoxal is a mutagenic product formed as secondary pollutant, through oxidation of hydrocarbons (Calvert *et al.,* 2000; Volkamer *et al.,* 2005; Volkamer *et al.,* 2001) and directly emitted from biomass burning and tailpipe emissions (Ban-Weiss *et al.,* 2008; Grosjean *et al.,* 2001; Hays *et al.,* 2002; Kean *et al.,* 2001), however when compared with secondary formation pathways, contribution from direct emissions were observed as minor (Fu *et al.,* 2008; Volkamer *et al.,* 2005).

2.5.1. Glyoxal in Atmosphere

Glyoxal is precursor of formaldehyde that has carcinogenic nature. Many studies have reported tropospheric glyoxal. For example, Munger and Lee along with their coworkers, reported the mean mixing ratios for glyoxal of 0.04 ppb_V and 0.07 ppb_V order respectively, in a rural site's boundary layer, originating from biogenic sources, i.e. isoprene (Lee *et al.,* 1998; Munger *et al.,* 1995). Lower glyoxal values of 0.03 ppb_V were reported over pine farm in California (Spaulding *et al.,* 2003). Glyoxal along with other aldehydes were detected in the air affected by burning of biomass, residential and domestic log fires (Ho & Yu, 2002).

2.5.2. Sources of Glyoxal

Glyoxal have 45 Tg a^{-1} of emissions globally, among these biogenic hydrocarbons oxidation is responsible for 55%, burning of biomass for 20%, emissions

from biofuel burning for 17%, and solely anthropogenic pollution sources for 8%, respectively (Fu *et al.,* 2008). From biogenic sources of glyoxal, primarily isoprene and up to some extent monoterpenes dominate. Isoprene is released during photosynthesis to release heat stress. Rate of isoprene emissions is directly dependent on the external temperature. Isoprene, being the most dominant source of most of existing NMVOC (non-methane VOC), accounts for about 65-70% of total glyoxal emissions (Fu *et al.,* 2008; Myriokefalitakis *et al.,* 2008; Vrekoussis *et al.,* 2009) and 44% of total VOC flux in the troposphere (Guanther *et al.,* 1995).

2.5.2.1. Biogenic Sources

Most important precursor of glyoxal is isoprene, contributing up to 47% of glyoxal globally. Oxidation by NO3 yields large quantities of glyoxal at cost of fractional loss of isoprene itself. Oxidation by OH radical produces glyoxal as secondary pollutant and also tertiary pollutant via glycolaldehyde ($HOCH_2CHO$) as intermediate. Globally glycolaldehyde contributes for 9.9% molar yield of glyoxal. During the periods when NOx concentrations are low, glyoxal production process can be delayed even for days. Global isoprene emissions from biogenic sources assessed by MEGAN are 410 Tg a^{-1}, generating about 21 Tg a^{-1} of glyoxal (Guenther, 2006). Glyoxal is also produced during oxidation of numerous monoterpenes with ozone, including geraniol, citral, D_3–carene and α-pinene (Fick *et al.,* 2004; Fick *et al.,* 2003; Nunes *et al.*, 2005). A-pinene accounts for glyoxal molar yield of about 4%-9%, this production is found to be sensitive to relative humidity and temperature (Fick *et al.,* 2004; Fick *et al.,* 2003). According to GEIA inventory global monoterpene emissions are 160 Tg a^{-1} and on average global glyoxal molar yield from monoterpene oxidation is 2.8%, generating 1.8 Tg a^{-1} of glyoxal (Guenther *et al.,* 1995). Glyoxal is also produced when aromatic compounds react in abiotic conditions in the presence of hydroxyl and ozone. Photochemical reactions of humic acids in sea water also results in glyoxal production (Mopper & Stahovec, 1986).

2.5.2.2. Anthropogenic Sources of Glyoxal

Among the anthropogenic emission sources acetylene (HC-CH) is the most important precursor and second major glyoxal source (Xiao *et al.,* 2007). It is released during combustion activity and against OH oxidation it has mean global lifetime of 18 days. Since acetylene has longer lifetime, it provides free sources of glyoxal and SOA

in troposphere, accounting for 20% of the total sources of glyoxal (Bohn & Zetzsch, 1998). Aromatic compounds also produce glyoxal during first stages of OH oxidation in ring cleavage reactions (Volkamer *et al.,* 2001). Several studies have reported that direct biomass and biofuel burning emissions produces glyoxal and its precursor glycolaldehyde (Christian *et al.,* 2003; Greenberg *et al.,* 2006). Automotive emissions and successively formed photochemical smog results in the formation of tropospheric glyoxal (Pitts *et al.,* 1985). In addition, Residential and domestic log fires are among the potential sources of glyoxal (Kleindienst *et al.,* 1986; McDonald *et al.,* 2000). Cigarette smoke emissions have been found to contain traces of glyoxal (Moree-Testa & Saint-Jalm, 1981). Ozone when used as water disinfectant reacts with organic carbon in the water to produce glyoxal (Lopez *et al.,* 1999).

Total anthropogenic glyoxal concentrations of 60% are produced by oxidation of acetylene driven by primary glyoxal concentrations of 20% and aromatic contributing about 15%. Glyoxal concentrations emitted by biogenic sources are considered secondary sources, where isoprene oxidation is responsible for 90% of total emission and remaining is contributed by monoterpenes and ethene. Sinks of glyoxal associated with in cloud SOA formation (4.7 Tg annually) are reported as in fair agreement with literature studies with the preceding estimate (Fu *et al.,* 2008). Though aerosols with irretrievable uptake, accounting for 5.9 Tg annually of organic carbon and black carbon and 1.8 Tg annually on sulfates, are found to be much higher than studies conducted by Fu and his coworkers on global budgets of Glyoxal (Stavrakou *et al.,* 2009). The resulting average lifetime opposite to SOA conversion (ca. 11 h), is found to be two times less than in comparison to the study reported by Fu (Fu *et al.,* 2008). Lifetimes in contradiction of photolysis and hydroxyl oxidation are found to be 4.8 h and 14 h, respectively, which are in fair agreement with Myriokefalitakis (Myriokefalitakis *et al.,* 2008). It was testified that sinks of glyoxal aerosol are significantly higher when the uptake coefficient from study conducted by Volkamer (Volkamer *et al.,* 2007), taken as 3.7×10^{-3} and total annual estimated concentrations are 9.2 Tg.

2.5.3. Removal Processes of Glyoxal

Several processes help to remove glyoxal from air naturally. Photolysis acts as the most prominent sink (Tadić *et al.,* 2006). Other sinks include SOA formation

(Volkamer *et al.,* 2007), dry and wet deposition (Fu *et al.,* 2008), and oxidation mechanisms driven by OH radical (Setokuchi, 2011).

2.5.3.1. Photolysis

Photolysis is the most important removal process of a variety of carbonyls and other pollutants during day time. Atmospheric residence time with respect to photolysis is of few hours (Tadić *et al.,* 2006). Theoretically photolysis of glyoxal can be shown as follows;

$$CHOCHO + h\nu \longrightarrow 2HCO$$

$$\Delta H^{o}_{298} = 68.5 \text{ kcal/mol}; \lambda_{threshold} \leq 417 \text{ nm}$$

$$CHOCHO + h\nu \longrightarrow H_2 + 2CO$$

$$\Delta H^{o}_{298} = -2.1 \text{ kcal/mol; all } \lambda$$

$$CHOCHO + h\nu \longrightarrow H_2CO + CO$$

$$\Delta H^{o}_{298} = -1.7 \text{ kcal/mol; all } \lambda$$

$$CHOCHO + h\nu \longrightarrow H + CO + HCO$$

$$\Delta H^{o}_{298} = 85.4 \text{ kcal/mol}; \lambda_{threshold} \leq 334 \text{ nm}$$

2.5.3.2. Wet and Dry Deposition

Due to higher water solubility potential, glyoxal may also be engaged by cloud droplets and aqueous aerosols, resulting in deposition (Betterton & Hoffman, 1988; Zhou & Mopper, 1990).

2.5.3.3. SOA Formation

Glyoxal potentially contributes for SOA formation as a precursor. It is found as an in-cloud precursor of carboxylic acids formation in atmosphere (Chebbi& Carlier, 1996). C-C bonds of carbonyls breaks in gas phase oxidation to yield, more volatile, smaller chemical species (Atkinson *et al.,* 2006).

2.5.4. Atmospheric Residence Time

Glyoxal has short chemical life time depending upon photolysis and reaction with OH radical (Atkinson, 2000; MacDonald *et al.,* 2012), it has average life time of 1-2 hours in troposphere and boundary layer, determined by the brightness of overhead sun (Volkamer *et al.,* 2005), and 2–3 hours worldwide (Fu *et al.,* 2008; Myruokefalitakis *et al.,* 2008).

2.5.5. Health Effects of Glyoxal

Glyoxal is a skin irritant, eye irritant and sensitizer as well. Direct contact with chemicals containing glyoxal can cause contact dermatitis Kielhorn *et al.,* 2004).

2.5.5.1. Carcinogen potential of Glyoxal

Glyoxal is found as direct genotoxic *in vitro* in mammalian and bacterial cells, it is also found to form DNA adducts, causing mutations, DNA repair, DNA single strand breakings, chromosomal aberrations and sister chromatid exchanges (Kielhorn *et al.,* 2004).

2.6. DOAS Technique

DOAS (Differential Optical Absorption Spectroscopy) being a remote sensing measurement practice allows the monitoring of trace gas species in atmosphere by using the structural absorption bands in visible and UV regions. It is one of the largely used spectroscopic monitoring. This instrument follows the difference principle in the absorption pattern of wavelengths. Using this method, trace gas species are recognized by absorption in their visible/Ultra Violet absorption band range. Few of relevant species include NO_2, O_4, CHOCHO, HCHO, H_2O, BrO, IO, O_3, and SO_2.

Lambert-Beer law is the ultimate principle for measurement of absorption cross-section, which states as; the decrease in EM radiation can be related with number of radiation absorbing molecules in optical path length,

i. $$I(\lambda) = I_o(\lambda)\, e^{-\alpha LC} \qquad (Eq.:2.i)$$

Where,

I: measured flux

I_o: incident flux

α: absorption cross section of the targeted species

L: Length of optical path

C: concentration of the absorbing trace gas (optical density).

Few of the limitations to Lambert Beer law are the presence of numerous gases, scattering phenomena and aerosols (including Rayleigh, Raman and Mie scattering). But still DOAS allows us to overcome these limitations partially, if not fully, particularly the scattering phenomenon and few instrumental impacts. Figure 2.6.1 illustrates the DOAS Principle.

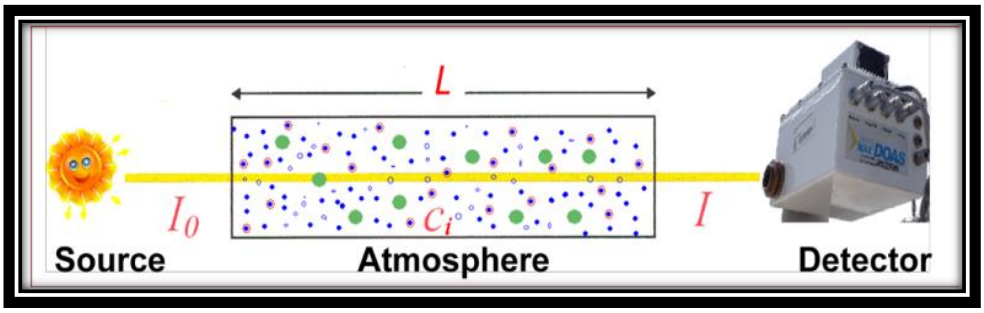

Figure 2.6.1: Pictorial view showing DOAS working Principle

Bookkeeping to scattering procedures, due to trace gas presence, the DOAS principle equation turns out to be:

$$I(\lambda) = I_0(\lambda)\cdot\exp\left(-\int_0^L\left(\varepsilon_R(\lambda,l)+\varepsilon_M(\lambda,l)+\sum_i\sigma_i(\lambda,p,T)\cdot c_i(l)\right)dl\right) \quad \textit{(Eq.:2.ii)}$$

$I(\lambda)$: Intensity of light after passing through atmosphere

$I_o(\lambda)$: Intensity of the light source

λ: Wavelength of absorption

$\varepsilon_R(\lambda, l)$: Coefficient of Rayleigh scattering

$\varepsilon_M(\lambda, l)$: Coefficient of Mie scattering

$\sigma_i(\lambda, p, T)$: Cross-section of the absorbing specie (i) for absorption

$c_i(l)$: Absorbing specie's (i) concentration

p: Pressure

T: Temperature

L: Total length of optical path

This broad-band absorption triggered through scattering phenomenon is not easy to quantify, so, the DOAS method splits the absorption cross-sections of trace gas in 2 different fragments.

$$\sigma(\lambda) = \sigma_b(\lambda) + \sigma'(\lambda) \qquad \textit{(Eq.:2.iii)}$$

σ_b: Scattering and broad-band absorption characterization

σ': Differential absorption cross-section

This defines representative absorption of thin band assemblies of trace gas specie. With the following principle, exponent value in law divided into 2 different parts: firstly, that one which varies gradually integrating broadband absorption and its scattering with the wavelength, while the other one presenting strong and significant reliance on wavelength because of narrow-band of the absorption of trace gas. So, now we can write the Beer-Lambert Law as follows:

$$I(\lambda) = I_0(\lambda) \cdot \exp\left(-\int_0^L \left(\varepsilon_R(\lambda,l) + \varepsilon_M(\lambda,l) + \sum_i \sigma_{b,i}(\lambda) \cdot c_i(l) \right) dl \right)$$

$$\cdot \exp\left(-\int_0^L \left(\sum_i \sigma_i'(\lambda) \cdot c_i(l) \right) dl \right) \qquad \textit{(Eq.:2.iv)}$$

Trace gas species absorption causes broad-band and narrow extinction, while Rayleigh and Aerosol scattering only shows broad-band scattering.

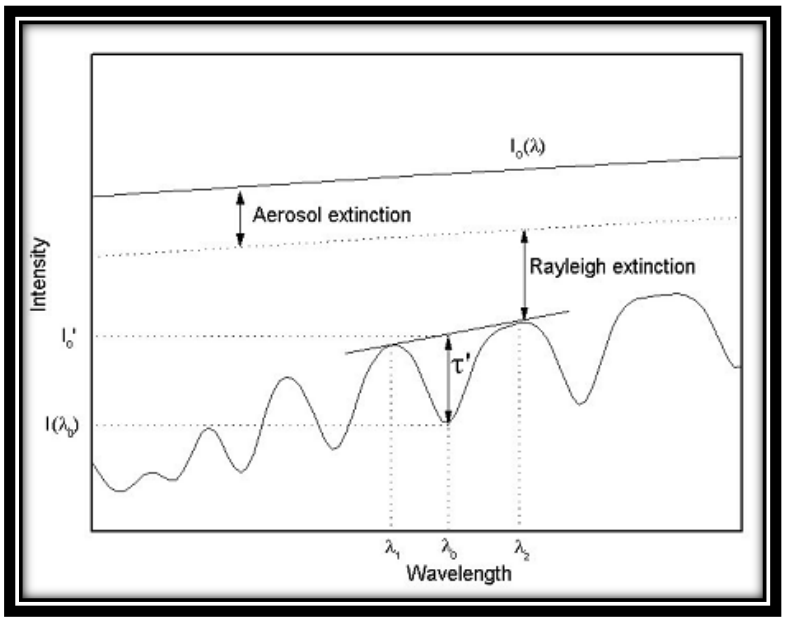

Figure 2.6.2: Radiation attenuation process in atmosphere

To get the differential base line intensity I_0', broad-band portion of the Eq.: 2.iv is fused with initial intensity of light as I_0

$$I_0' = I_0(\lambda)\cdot\exp\left(-\int_0^L\left(\varepsilon_R(\lambda,l)+\varepsilon_M(\lambda,l)+\sum_i\sigma_{b,i}(\lambda)\cdot c_i(l)\right)dl\right) \quad \textit{(Eq.:2.v)}$$

So The Beer-Lambert Law can now be expressed in the following differential form.

$$\tau'(\lambda) = \ln\left(\frac{I_0'(\lambda)}{I(\lambda)}\right) = \int_0^L\left(\sum_i\sigma_i'(\lambda)\cdot c_i(l)\right)dl \quad \textit{(Eq.:2.vi)}$$

$\tau'(\lambda)$: Differential optical density

This differential optical density reflects the result of DOAS technique.

2.6.1. Glyoxal Detection in Air

First ever reported direct stratospheric measurements of glyoxal were detected with concentrations up to1.8 ppb_V, in Mexico City as photochemical product of second

order in Road side traffic emissions, though directly measured traffic emissions were far smaller (<4%) (Volkamer *et al.,* 2005).

A comparative study was done in South East Asia tropical rain forest using MAX-DOAS and LP-DOAS to determine glyoxal and formaldehyde and a significant photochemistry was observed over the rain forest. Results showed that glyoxal was found more abundant above the forest covering in comparison to any country side environment and glyoxal was found restricted in boundary layer, mainly within the first 500m of the BL. According to them the most significant pathway of glyoxal formation was oxidation of isoprene by OH radical and surprisingly, measured glyoxal levels were found consistent with OH concentrations present in that environment (MacDonald *et al.,* 2012).

Glyoxal was detected by passive MAX-DOAS in ICARTT campaign (International Consortium for Atmospheric Research on Transport and Transformation) at MIT Cambridge, USA, in 2004 and in Gulf of Maine, on board the research vessel Ron Brown. Optical densities of up to 3.5×10^{-3} were detected using fit window of 420-460 nm. Heights of planetary boundary layer and mixing ratios there in were also calculated at each side, on a clear day, by using radiative transfer models. Mixing ratios measured at MIT were found varied from 40-140 ppt whereas at Ron Brown measured values were three times greater than MIT (Sinreich *et al.,* 2007).

Glyoxal detection is feasible using passive DOAS applications consuming solar light in MAX-DOAS and space born DOAS. These measurements act as very important indicator species for atmospheric VOC chemistry. Glyoxal is also responsible for smog formation, during VOC oxidation reactions in morning and overhead sun conditions. Since glyoxal can be used to predict photochemical smog formation using photochemical prediction models (Volkamer *et al.,* 2005).

Atmospheric glyoxal columns were retrieved with DOAS method using satellite observations from OMI spectrometers and high levels of glyoxal were observed over regions polluted with pyrogenic and biogenic emissions. Areas with more anthropogenic activities were identified as hot-spots. Using the OMI spectrometers pyrogenic activities were identified over Russia for wildfires during July and August, 2010 and Africa (Alvarado *et al.,* 2014).

CHAPTER 3

DATA SETS AND METHODOLOGY

3.1. Mini Max-DOAS Instrument

The instrument mini-MAD-DOAS is a fully automated, light weight spectrophotometer with dimensions of 13cm × 19cm × 14cm. Instrument contains electronically controlled spectrograph coupled with fibers. Within the instrument light is dispersed by an intersected Czerny-Turner spectrometer (Ocean Optics Inc., USB2000+), using quartz lens of 40 mm focal length present at the entrance of optics, using one dimensional CCD detector (Sony ILX511, 2048 individual pixels). Viewing angle elevation is being controlled by rotating the instrument between the horizontal and vertical using a stepper motor. Spectral range of the instrument is from 320 nm to 460 nm with 0.7 nm resolution. Mini-MAX-DOAS can be operated on desktop or laptop having XP Window operating system, installed with DOASIS software. The instrument can also be used for field campaigns, as it can scan air while tied up on moveable platform (Kraus, 2006).

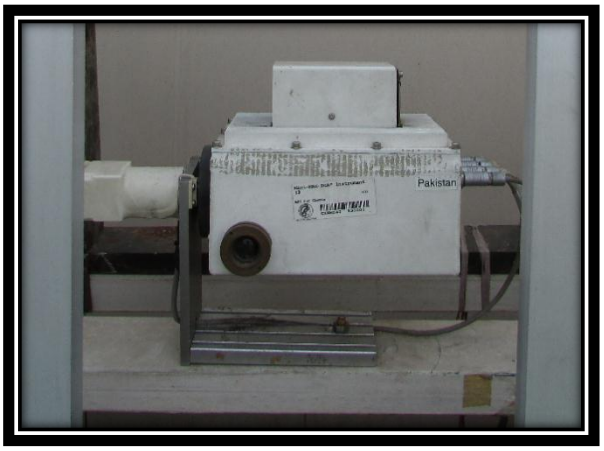

Figure 3.1: Mini-MAX-DOAS instrument mounted at roof top of IESE-NUST building in Atmospheric Research Laboratory

3.2. Site Description

3.2.1. Site A: IESE-NUST

Institute of Environmental Sciences and Engineering (IESE), is situated at Islamabad (33.6416° N, 72.9835° E), Pakistan. The instrument was mounted on the roof top of the two story building (referred as Air Research Lab, IESE-NUST, in this study and shown by red balloon in Figure 1) pointing towards the South. In its vicinity

Kashmir Highway is passing by its North side, Grand Trunk road on South West and IJP road on the South side. All of these roads cater major mutability of both light and heavy vehicles passing through and within the twin cities of Islamabad and Rawalpindi. The Rawalpindi city is situated at southeast side of the IESE-NUST – the fourth most populated city (population of 2.16 million) of Pakistan with relatively poor air quality as compared to Islamabad (population of 0.9 million).

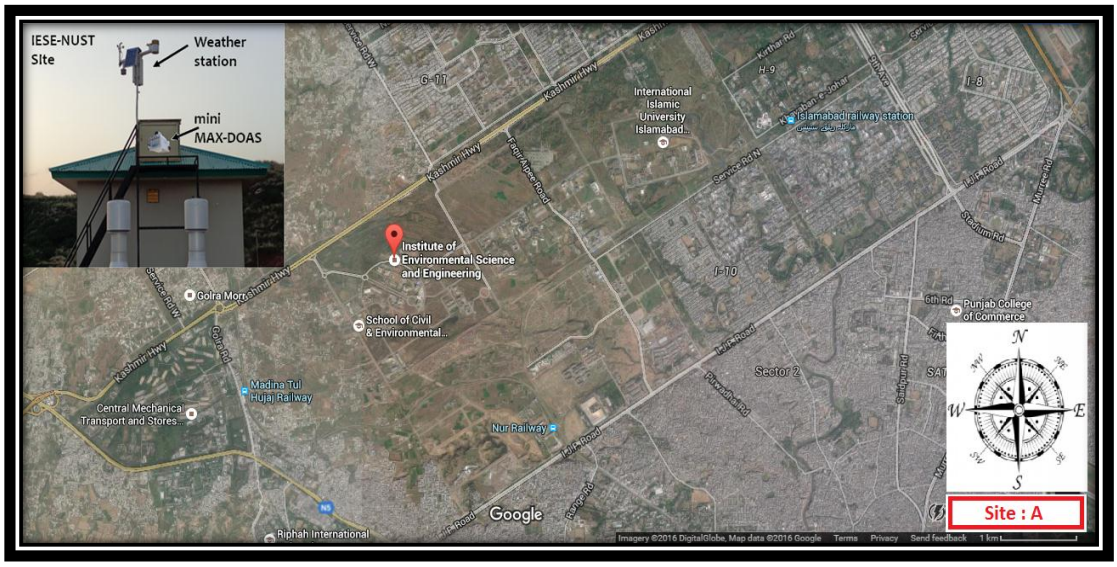

Figure 3.2.1: Red balloon is showing the location of mini MAX-DOAS instruments deployed at IESE-NUST site in Islamabad, Pakistan

3.2.2. Site B: MPI-Ch

The other selected site, MPI-Ch building is situated (49.965387° N, 8.242531° E) at Mainz, Germany as shown by red balloon in Figure 1. The instrument was deployed on a five story building with Saar street main road on the North side and Koblenzer street road on the West side. The North is densely populated side (Wiesbaden city with approximate population of 280,000), East and South side (Mainz City) have population of 200,000 while open fields exist on West side.

Figure 3.2.2: Red balloon is showing the location of mini MAX-DOAS instruments deployed at MPI-Ch building Mainz, Germany

3.3. Measurements at MPI-CH, Mainz, Germany Site

The MAD-CAT campaign was conducted at the Max-Planck Institute für Chemi, a semi-urban zone in Mainz, Germany. Though the main focus of field campaign was to monitor several trace gases and aerosols with the in-situ systems, but the sun photometers were also installed and other meteorological parameters as ambient temperature, precipitation, relative humidity, wind speed and direction were also monitored.

Sixteen different instruments from eleven institutions (NUST Islamabad, Pakistan; MPIC, Mainz Germany; University of Heidelberg, Germany; University of Bremen, Germany; CAMS Beijing, China; CAS Hefei, China; IISER Mohali, India; University of Galati, Romania; University of Colorado Boulder, USA; University Minsk, Belarus; BIRA/IASB Brussels, Belgium), were deployed and tested between 7th to 16th June 2013. And an initial inter-comparison for glyoxal DSCDs retrieval assisted to confirm the instrumental and DOAS fit settings, to be used for further glyoxal analysis, as stated in segment 2.6. The monitoring continued till 17th July 2013 while other species such as NO_2, HCHO, BrO, O_4 etc. were also focused. This initial inter-comparison was designed to check the reliability of different multi-axis instruments used in MAD-CAT field campaign. Instruments collected the scattered light spectra by the set of suggested elevation angles (2, 4, 8, 15, 30, 45, 75 and 90) with 1-2 minutes' integration time. One whole prescribed set of elevation angles were being retrieved within 10-20 minutes.

3.4. Measurements at IESE-NUST Site

Selected time period for measurement was from October 2014 to September 2015. The scattered spectra of light were retrieved by the set of prearranged elevation angles (2, 4, 5, 6, 10, 15, 30, 45 and 90). Individual measurement interval was about one minute, and it took about nine minutes to complete the cycle.

3.5. Software

Software used for the retrieval of glyoxal VCDs from data are listed in table 3.1.

Table 3.1: Software used in the study, their versions and respective Tasks

Sr. #	Software	Version	Tasks
1	DOASIS (Differential Optical Absorption Spectroscopy Intelligent System)	Version 3.2.350	Operating Software for MAX-DOAS and measurement of back scatter intensities
2	WinDOAS (Windows Differential Optical Absorption Spectroscopy)	Version 2.1	Calibration
2	QDOAS (Q Differential Optical Absorption Spectroscopy)	Version 2.110.1	Analysis of UV-Visible Spectra by DOAS to retrieve DSCDs
3	Microsoft Excel	Microsoft Office 16	Mathematical Calculations for tropospheric VCD extraction and Graphical representations

3.5.1. DOASIS

DOASIS (Differential Optical Absorption Spectroscopy Intelligent System) operates the MAX-DOAS and records the measured spectra. Its functions include, controlling the spectrometer temperature, stepper motor and integration time per spectrum. Figure 3.2 is showing pictorial view of DOASIS while taking spectrum.

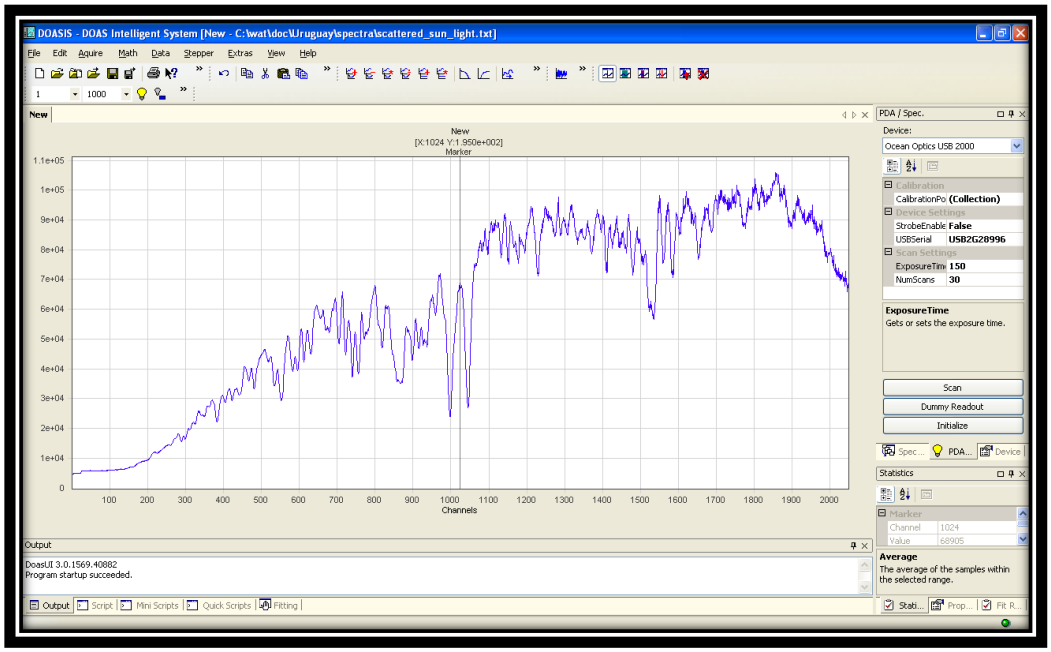

Figure 3.2: Pictorial view of DOASIS Window

DOASIS is used to calculate dark current, offset and Ring spectrum for spectrometer, all of these are used in DOAS fit analysis in later steps. Dark current and offset are used for zero correction of measured spectra. Offset being the spectrum measured in dark and to measure it, high scan number is used for a small integration time (e.g. 1000 scans per 3 milliseconds). Whereas, Dark current being the smaller electric current flowing through DOAS spectrometer and to measure it, small scan number with moderate integration time is used (e.g. 1 scan per 10,000 milliseconds).

Slant column densities of glyoxal were retrieved from measured spectra using QDOAS software (Q Differential Optical Absorption Spectroscopy) (Danckaert *et al.*, 2015). And for calibration of wavelength, a solar spectrum with high resolution was used in WinDOAS (Kurcuz *et al.*, 1984).

For glyoxal 322.5-360 nm wavelength analysis window was chosen. For DOAS fit absorption trace gas cross section used were; glyoxal (Volkamer *et al.*, 2005), NO_2 (io, 1×10^{17} molecules/cm^2, 298 K) and NO_2 (220K) (Vandaele *et al.*, 1998), O_3 (223K) (Bogumil *et al.*, 2003) O_4 (293K) (Thalman & Volkamer, 2013), H_2O (296K, HITEMP) (Rothman, 2010), Ring (Ring_NDSC2003) and online convolution of these cross sections were done with constant offset and fifth order polynomial degree in the fitting process of QDOAS.

For glyoxal analysis, WinDOAS and QDOAS were used in the following three major steps:

- Wavelength Calibration
- Wavelength Convolution
- Glyoxal Analysis

1.5.2. WinDOAS

1.5.2.1. Wavelength Calibration

The calibration process is done using a measured spectrum fitted to a convoluted solar spectrum. A noon spectrum of high intensity is used for this purpose.

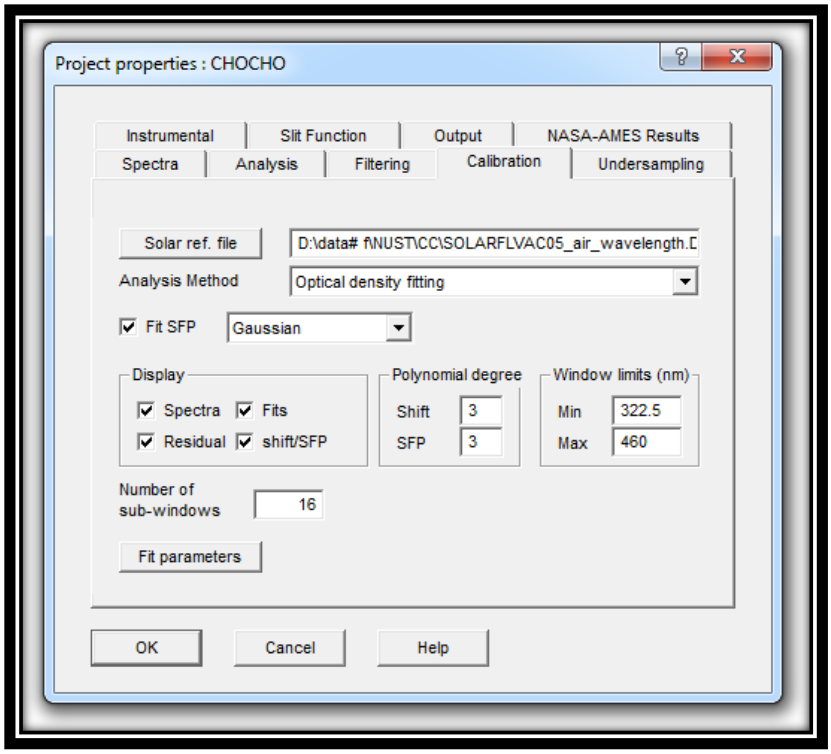

Figure 3.3: WinDOAS Calibration Window showing the specifications used for calibration

Calibration fit is often referred as "Kurucz-fit" since it uses a spectrum with high resolution as input and convolutes it accordingly as per the mini-MAX-DOAS's spatial resolution. Whole wavelength is divided into numerous sub-windows. To reduce the residual error in the calibration process, calibration is repeated twice. At the end this calibrated spectrum is used to analyze all measured spectra in QDOAS.

1.5.3. QDOAS

3.5.3.1. Wavelength Convolution

The convolution of a spectrum *I* by an instrumental slit function *F* is given by the integral

$$(F * I)(\lambda) = \int I(\lambda')F(\lambda - \lambda')\mathrm{d}\lambda\,. \qquad \text{(Eq. 3.1)}$$

In QDOAS, width of the slit function defines the integration interval *F* and it is calculated using the trapezoidal rule. Convoluted cross section fitting to the measured optical depth by the low resoling instrument depend upon approximation.

Accordingly, the fitting of a convolved cross sections to the measured optical depth depend on an estimate. This estimate determines the error depending upon the strength of adsorption and the relation of the width of slit function and spectral structures in the cross section S_o and the light source I_o.

In case of present study, online convolution was done. Several trace gas cross-sections were used as stated in Table 3.1. Along with these, Gaussian shape was used as slit function with 0.7 nm FWHM.

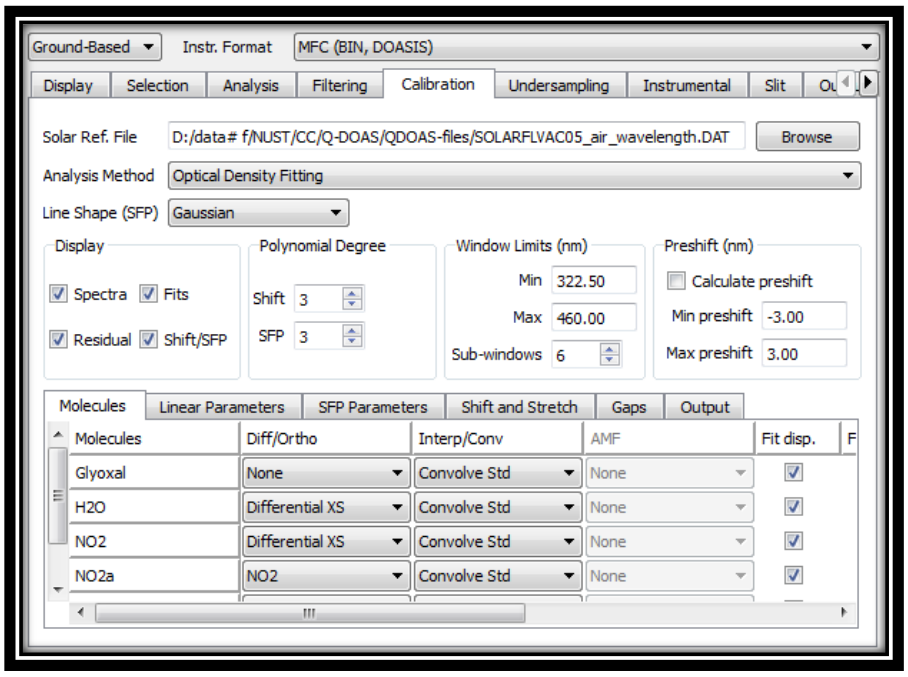

Figure 3.4: QDAOS Convolution Window showing specifications used for on line convolution

3.5.3.2. Glyoxal Analysis Window

In case of glyoxal wavelength range of 415 - 461 nm was used after various run and the lowest possible fit error residual. Here for the analysis, reference spectrum used is the calibrated spectrum, created previously in WinDOAS.

DOAS technique is widely used for the retrieval of trace gases in the boundary layer and troposphere (Platt & Stutz, 2008). Being a self-calibrating technique it identifies the structure of absorption molecules allowing the various trace gas retrievals simultaneously within designated wavelength interval. Taking in account the related absorption cross sections of each trace gas, retrieved spectral signature of the gas are then transformed to SCDs (slant column densities). MAX-DOAS technique was specifically developed for the retrieval of information about trace gases having shorter life time, from the observations accompanied for the lower angles of elevation (Friβ *et al.*, 2006; Heckel *et al.*, 2005; Hönninger *et al.*, 2004; Leser *et al.*, 2003; Sinreich *et al.*, 2007; Roozendael *et al.*, 2003; Wittrock *et al.*, 2004).

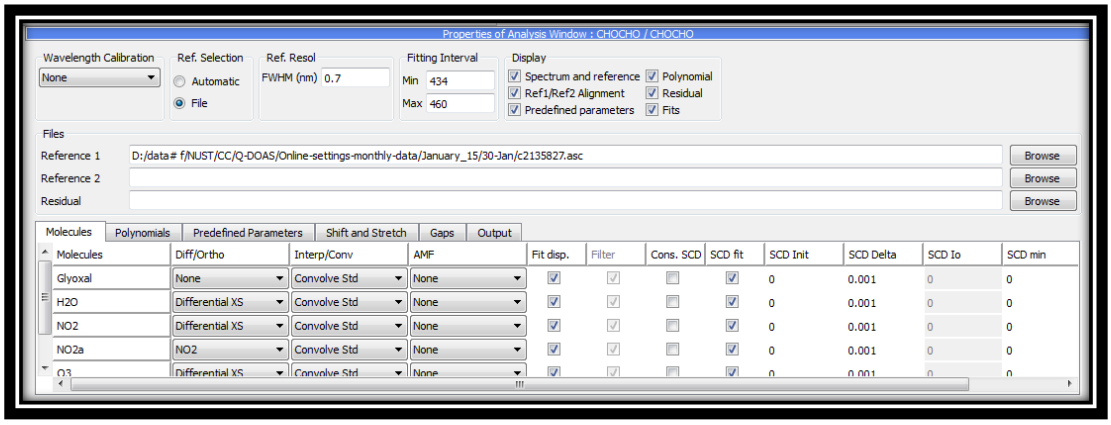

Figure 3.5: QDAOS Analysis Window showing specifications used for analysis

3.5.4. Microsoft Excel

QDOA's results are automatically saved as ASCII file, on the given assigned path in computer and later on those files are opened as Delimited; Space; General file in MS Excel. An example of MS Excel type, QDOAS output file is shown in fig. 3.6.1.

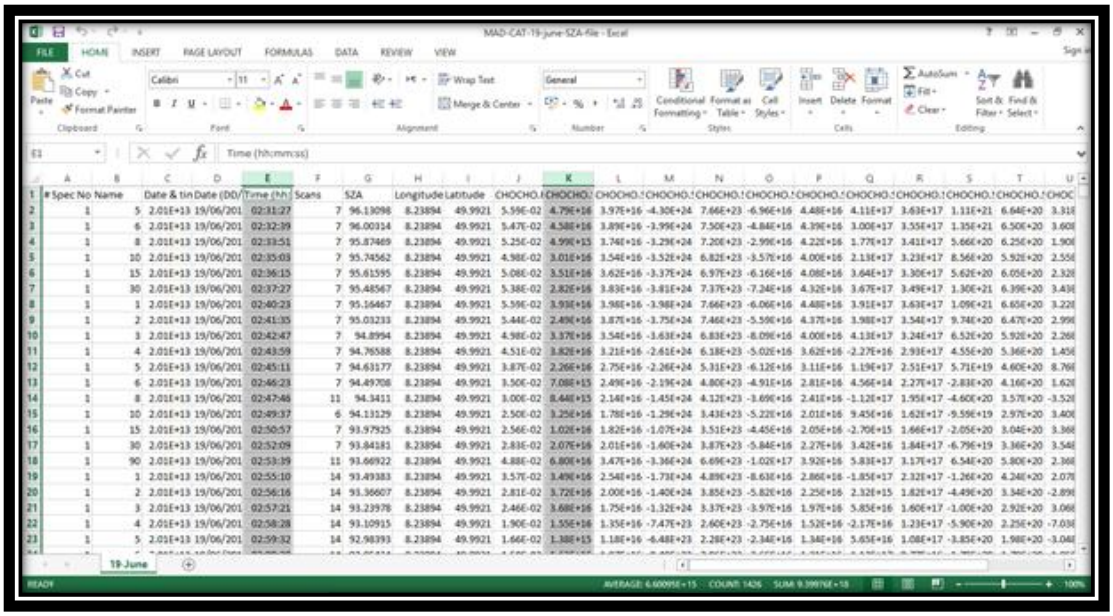

Figure 3.6.1: Microsoft Excel Window showing glyoxal Root Mean Squares (RMS) and glyoxal (DSCD) values

3.6. Glyoxal Retrieval Process

The glyoxal DSCDs were obtained by applying DOAS fitting method (Platt & Stutz, 2008; Sinreich *et al.*, 2007) to the retrieved spectra (Fayt & Roozendael, 2001). DSCDs we retrieve as output in the form of ASCII files are basically the difference between SCDs (measured at 30°elevation angle) and the selected reference spectrum (it is a Fraunhofer reference spectrum taken at minimum SZA; $\alpha = 90°$). Function of this Fraunhofer reference spectrum is to auto correct the measured spectra for resilient Fraunhofer absorption lines present their in. To retrieve the best glyoxal DOAS fit several test runs of optimal fit settings (e.g. wavelength range, polynomial degree, instrumental slit functions, selection of the best cross-sections, etc.) were carried out by all the scientists contributed in MAD-CAT campaign. By applying shift and stretch, measured spectra were then adjusted against the selected Fraunhofer reference spectrum and fitted cross sections.

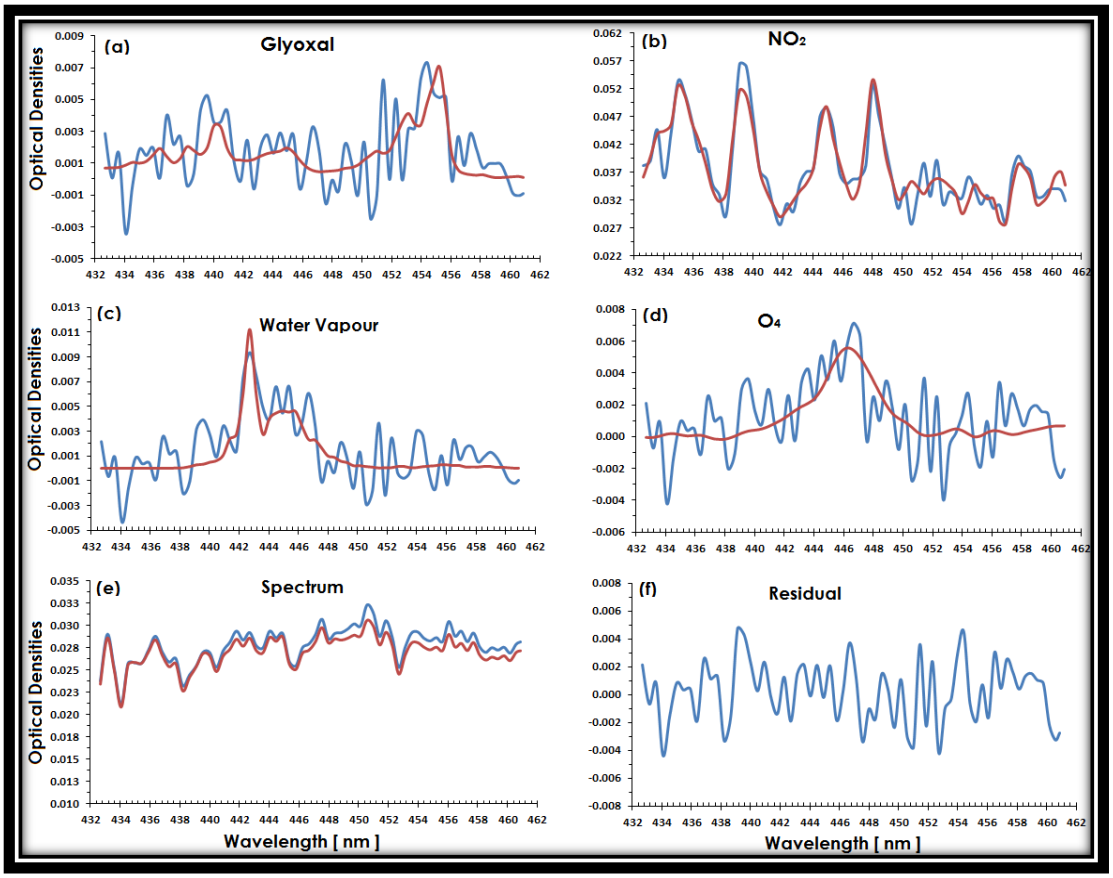

Figure 3.6.2: Showing an example of glyoxal DOAS fit applied to the measured spectrum on 26th June 2013 (MAD-CAT, Germany), 2:17 PM at elevation angle of 5 ($\alpha = 5°$). Red lines signify the optical densities of the measured cross-sections and blue lines indicate the sum of residual and measured cross-sections as a function of wavelength, **(a)** glyoxal, **(b)** NO_2, **(c)** water vapor, **(d)** O_4, **(e)** spectrum and **(f)** fit residual. Glyoxal DSCDs retrieved for this spectrum was 1.3×10^{16} molecules/cm^2

Principally the glyoxal retrieval was largely obstructed by the Ring structures (rotational Raman scattering occurring on air molecules). Raman scattering tends stronger towards the smaller wavelengths therefore the retrieved DOAS fit showed comparatively good results for the suggested wavelength range at 434-460 nm. For this study, fit interval of 437-460 nm was used and the measured spectra were fitted against convoluted cross-sections of selected trace gases like; NO_2 at two different temperatures (220˚K and 298˚K), O_3, O_4, glyoxal, H_2O and two ring cross-sections. Logic behind the use of two different NO_2 absorption cross sections was to avoid the possible error in glyoxal DOAS fit, which was mainly supposed to cause by inadequate removal of NO_2 absorptions. NO_2 certainly acts as a strong absorber in the selected wavelength interval. As it can lead to large biasedness in the glyoxal retrievals, because of its imprecise wavelength calibration and the temperature dependency of its absorption cross-sections. Besides, the reference spectrum for NO_2 and O_3 were also

corrected the solar I_0-effect. In order to limit the systematic errors in glyoxal retrieval, various sensitivity runs were carried out for wavelength interval (between 415 – 460 nm), polynomial degree (from 3 – 5), shift and squeeze. Though, the systematic error for retrieved glyoxal DSCDs varied between 15% to 40% for all compassion tests and is in line with the previously reported studies (Frieβ *et al.*, 2006; Heckel *et al.*, 2005; Hönninger *et al.*, 2004; Leser *et al.*, 2003; Li *et al.*, 2013; Platt & Stutz, 2008; Sinreich *et al.*, 2007; Roozendael *et al.*, 2003; Wittrock *et al.*, 2004).

The optimal settings used for glyoxal DOAS fit are enlisted in Table 3.6.1., in addition the specified settings used by several studies for glyoxal DSCDs retrieval, are also listed. Quantitative filtering of retrieved DSCDs was done by applying filter of 2.0×10^{-3} on RMS (root mean square) column in the excel sheet. An example of retrieved glyoxal DOAS fit is shown in Fig. 3.6.2.

The spectrum was measured on 26th June 2013 at 2:17 PM at 5° elevation angle for MAD-CAT site. For the retrieval process the reference absorption cross sections used are glyoxal (Volkamer *et al.*, 2005), O_3 (Bogumil *et al.*, 2003), NO_2 (Vandaele *et al.*, 1998), O_4 (Thalman & Volkamer, 2013), water vapor (Rothman, 2010). The red line exemplifies the scaled test references plotted against the optical densities and the residual in blue lines, as a function of fitted wavelength. The DOAS fit quality is presented by the RMS variation of the residual (Fig. 3.6.2.f). The calculated glyoxal DSCDs for this measurement were 1.3×10^{16} molecule/cm^2.

Table 3.6.1: List of set of few reported settings used for DOAS Fit and Residuals

S. No.	Study	DOAS fit Settings			DOAS Fit Residual
		Absorption Cross-Sections	References	Wavelength Range	
1	This study	NO_2(220,298K) O_3(223 K) O_4 Glyoxal H_2O (296K) Ring_NDSC2003	(Vandaele *et al.*, 1998) (Bogumil *et al.*, 2003) (Thalman & Volkamer, 2013) (Volkamer *et al.*, 2005) (Rothman, 2010) (Mo & Li, 1992)	434-460 nm	8×10^{-4} to 5×10^{-3}
2	(Li *et al.*, 2013)	CHOCHO H_2O NO_2 O_3(280 K) O_4	(Volkamer *et al.*, 2005) (Rothman *et al.*, 2005) (Voigt *et al.*, 2002) (Voigt *et al.*, 2001) (Greenblatt *et al.*, 1990)	415-440 nm	1×10^{-2} to 1×10^{-3}
3	(Coburn *et al.*, 2011)	O_3(223 K) NO_2(294 K) O_4 CHOCHO H_2O, Ring	(Bogumil *et al.*, 2003) (Vandaele *et al.*, 1998) (Hermans) (Volkamer *et al.*, 2005) (Rothman *et al.*, 2005)	434-460 nm	6×10^{-5} to 1.4×10^{-4}
4	(Sinreich *et al.*, 2007)	NO_2 O_3 (223 K) O_4, CHOCHO, H_2O	(Vandaele *et al.*, 1998) (Bogumil *et al.*, 2003) (Greenblatt *et al.*, 1990) (Volkamer *et al.*, 2005) (Rothman *et al.*, 2005)	420–460 nm	1.4×10^{-3}

Using the suggested settings analysis was performed. For each day a Fraunhofer reference spectra with lowest SZA around local noon was used as reference to run analysis in QDOAS. From the retrieved DSCDs tropospheric glyoxal VCDs were calculated using the differential air mass factor method (It is the difference of air mass factor (AMF) between $\alpha = 90^{\circ}$ and $\alpha \neq 90^{\circ}$). AMF calculation using radiative transfer modeling is dependent upon several factors like, viewing geometry, cloud fraction, surface albedo, aerosol loading and previous profile of trace gas absorber (Hendrick *et al.*, 2006; Wanger *et al.*, 2007). Practically we often do not have information about all these parameters. Still, this can be done using geometric approximation (Sinreich *et al.*, 2007) given by Equation 3.6.1.

$$VCD_{geo} = \frac{DSCD_{(\alpha)}}{DAMF_{(\alpha)}} = \frac{DSCD_{(\alpha)}}{(1/\sin_{(\alpha)} - 1)} \quad \rightarrow \quad \text{Eq. (3.6.1)}$$

Where;

α : Elevation angle

and the indecisions (mostly introduced by spatial inhomogeneity of the absorber, aerosol load etc.) presented for NO_2 by this method are up to 20% (Pikelnaya *et al.,* 2007) and might not outstrip in the case of glyoxal retrieval as well (and we assume that due to shorter time span, it mostly exists in the boundary layer of troposphere and its concentrations in the semi-urban environments are found nearly homogeneously dispersed).

CHAPTER 4

RESULTS AND DISCUSSIONS

4.1. Comparison of June-July 2013 and 2015 for Site A and Site B

In the first part of results, comparison between outcomes of glyoxal VCDs was done using the two different data sets from two different time zones. One from Site A (referred as IESE-NUST, Islamabad Pakistan) for June-July 2015 and second from Site B (MAD-CAT campaign held in Mainz Germany) for June-July 2013.

4.1.1. Glyoxal Column Densities Measured Over IESE-NUST (June-July 2015)

An initial inter-comparison of glyoxal DSCDs for MAD-CAT data helped out for setting up the instrumental and DOAS fit settings, for further analysis of other data sets, as mentioned in section 3.6. Main objective of the initial inter-comparison was to check the reliability of involved multi-axis instruments in this campaign. And same settings were then used to retrieve glyoxal column densities of both data sets.

Figure 4.1.1 is representing glyoxal VCDs measured at 30° elevation angle at IESE-NUST monitoring site in Pakistan during the period of 18th June to 18th July 2015. Same settings for DOAS fit analysis were used as stated in earlier section 3.4 and Table 3.1. Maximum glyoxal VCDs of 7.81×10^{15} molecules/cm^2 were measured on 4th July 2015. Fluctuation in wind direction was observed between 80˚ to 220˚ N during this study period. In summer ambient air temperature in Pakistan may rise up to 45˚C or even more at the IESE-NUST monitoring site. However, calculated daily mean of glyoxal VCDs over IESE-NUST site are lower when compared with the daily mean VCDs from MAD-CAT site as illustrated in Figure 3.2.2. This difference in glyoxal concentration can explained by the observed difference in temperature variation of both monitoring sites. At Mainz, observed temperature has shown somewhat larger variations (from 11˚C - 36˚C) as compared to IESE Site (23˚C to 43˚ C). Particularly, the observed minimum ambient air temperature was 22.6˚ C at IESE-NUST site in 2015, in comparison to 11˚ C at MAD-CAT site in 2013.

Increase in air temperature causes enhanced emissions of isoprene and monoterpenes. So, the increased biogenic source contribution from isoprene and

monoterpenes can be expected at IESE site. So, ambient air temperature increases from 25°C - 35°C may cause increase in isoprene and monoterpene (Seinfeld & Pandis, 2012) emissions by a factor of 4 and 1.5, respectively (Lamb *et al.*, 1987). Though, more glyoxal has been observed at MAD-CAT site as it has more vegetation (see Figure 3.2.2) than IESE site (see Figure 3.2.1) and lesser actinic flux as it is located more towards north (Mainz 49.9˚ N) in comparison to Islamabad (i,e, located more towards south - 33.6˚ N).

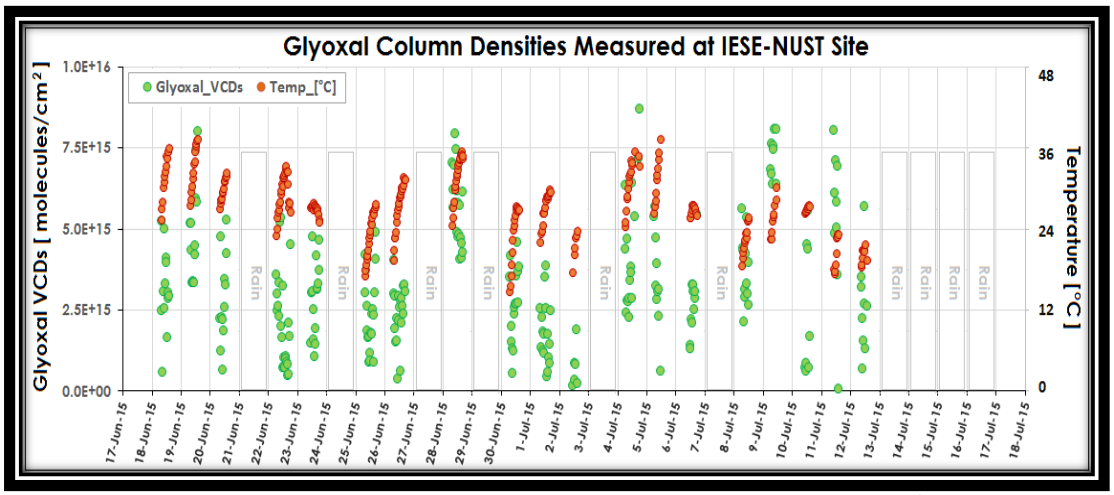

Figure 4.1.1: Showing Time series of glyoxal VCDs (molecules/cm^2) and ambient temperature (^{o}C), excluding the rainy day's data, measured at 30˚ elevation angle and averaged at interval of half an hour, at site A from 17th June - 18th July 2015.

4.1.2. Glyoxal Column Densities Measured during MAD-CAT Campaign (June-July 2013)

Figure 4.1.2 illustrates the glyoxal VCDs (molecules/cm^2) measured at elevation angle of 30° for site B from 18th of June - 18th of July, 2013. This time series cover up period of almost one month (in graphical representation days with instrumental malfunction and rain were excluded). Among the sixteen mini MAX-DOAS instruments, results of only the one from IESE, Islamabad, Pakistan will be discussed here. Glyoxal VCDs were compared with ambient air temperature, both for this both of these were averaged over time period of half an hour. Large scattering in glyoxal column densities was observed over the whole measuring period. And it can be seen that correlation between temperature variation over the day and the measured glyoxal VCDs is not so good. Although, main observed sources of glyoxal are dominated by oxidation of non-methane VOCs from biogenic emissions (i,e, isoprene/monoterpene). Though, ambient air temperature is not the only key factor of determining the diurnal variation in glyoxal concentration. In particular, large glyoxal

columns (1.4×10^{16} molecules/cm^2) were observed on 26th June 2013 for relatively lower temperature. An interesting feature of enhanced glyoxal VCDs were observed mainly during the wind direction around 270˚ N but independent of temperature. It is further conferred by the Figure 3.2.2 that in the upward wind direction (270˚ N) a forest site "Lenneberg Wald" is located and possibly acted as a potential source of glyoxal VCDs observed at MAD-CAT site. Metrological observation has revealed that the wind directions fluctuated between 245˚ to 320˚ N on most of the days all over the MAD-CAT campaign.

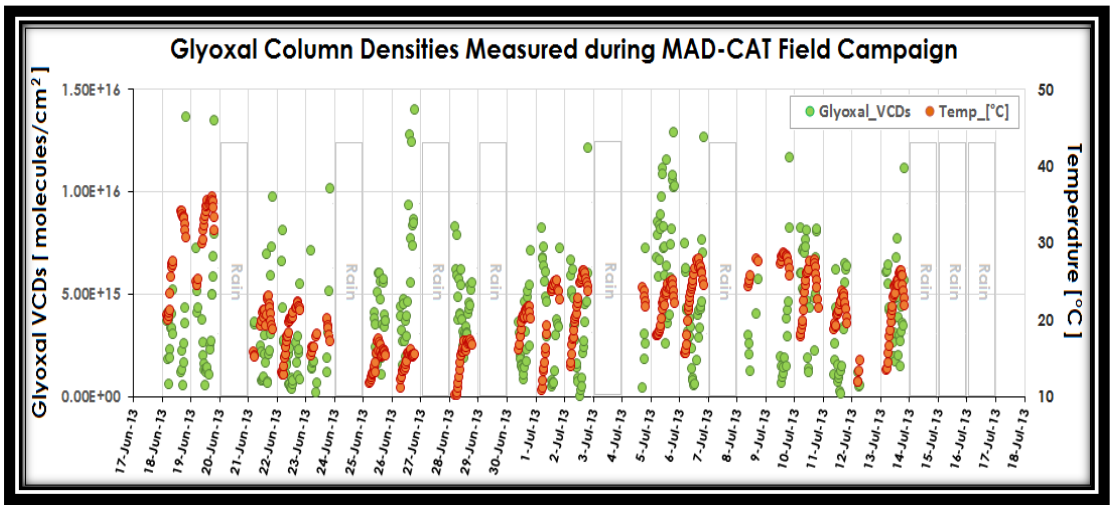

Figure 4.1.2: Showing Time series of glyoxal VCDs (molecules/cm^2) and ambient temperature (^{o}C), excluding some of the rainy day's data, measured at 30˚ elevation angle and averaged at interval of half an hour, at site A from 17th June - 18th July 2013.

4.1.3. Comparison of Daily Mean Glyoxal VCDs

In Figure 4.1.3. comparison of Glyoxal column densities measured at both monitoring sites (Site A: IESE-NUST, Islamabad, Pakistan and Site B: MAD-CAT, Mainz, Germany) are plotted for the period 18th of June to 13th of July. Data for 7th of July was missing during MAD-CAT campaign because of maintenance issue, so the measured glyoxal value for site A was also exclude from this graph.

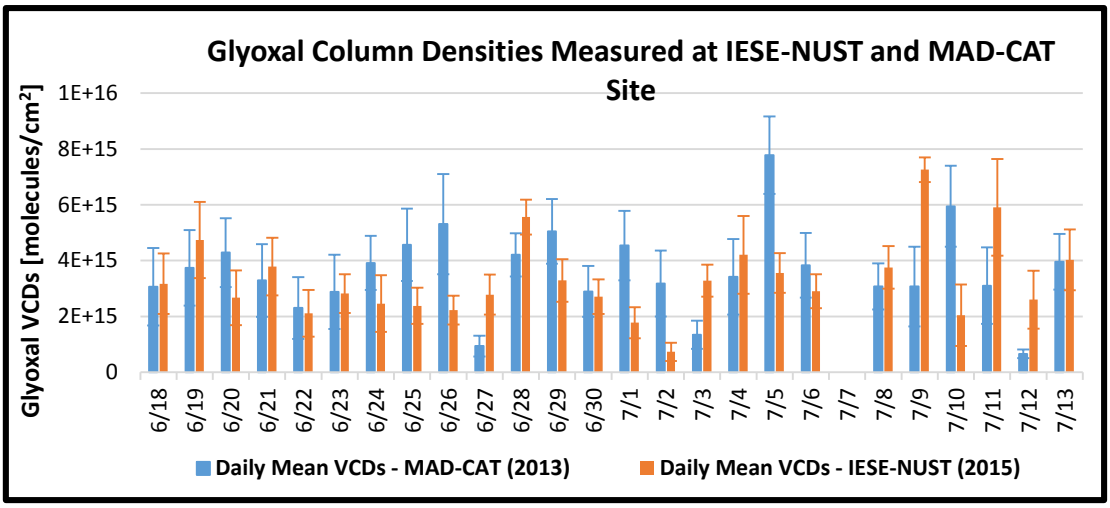

Figure 4.1.3: Showing the comparison of daily mean values of glyoxal VCDs (molecules/cm^2) retrieved at site A (in brown bars) and site B (in blue bars) for June and July 2015 and 2013 respectively.

4.1.4. Comparison of Glyoxal Diurnal Cycle

Enhanced glyoxal levels are found globally over the regions hosting VOC precursors from pyrogenic and mainly biogenic emissions (Alvarado *et al.*, 2014; Seinfeld & Pandis, 2012; Vrekoussis *et al.*, 2009) and uncertainties may exist as the emissions depends upon several parameters; such as vegetation type, humidity, temperature, wind speed and direction (Guenther *et al.*, 2000; Seinfeld & Pandis, 2012). Globally, hydrocarbon emission from anthropogenic sources are far less than those of biogenic (Seinfeld & Pendis, 2012). Photolysis being the major sink of glyoxal which is further followed by oxidation from OH radical and secondary organic aerosol formation (Liggio *et al.*, 2005).

Glyoxal concentration tends to decrease almost after one hour of sun rise and remains detectable for nearly most of the day time. A clear decreasing trend is observed in glyoxal emissions and can be attributed to higher photolysis rates near and after the local noon time (Volkamer *et al.*, 2005) followed by increasing concentrations in the evening hours (Myriokefalitakis *et al.*, 2008). Over both of monitoring sites similar trend in diurnal variations of glyoxal column densities was observed (see Figure 4.1.4 (a) and 4.1.4 (b)).

VOC oxidation by OH radicals available through the previous night and oxidation of isoprene/monoterpene causes the accumulation of glyoxal, in the atmosphere that is detected during morning hours (Li *et al.*, 2013). Followed by sight peak around 9:00-10:00 hours and can be claimed by anthropogenic emissions sources (i,e, emissions from vehicles particularly during morning rush hours). And at near solar

noon and afterwards, it shows a slight increase primarily caused by increased photo oxidation rate of isoprene/monoterpenes (Huisman *et al.*, 2011). Whereas in the evening hours glyoxal concentrations tend to increase and that can be claimed to the increased traffic emissions during evening rush hours and significant decrease in sunlight intensity (Sinreich *et al.,* 2007).

Relative humidity has anti-correlation with temperature and changes it with the change in temperature. And temperature has positive correlation with actinic flux, as it increases with increase in actinic flux. Therefore, the impact of temperature, actinic flux and relative humidity are investigated over both sites according to the respective data sets. Interestingly, over both monitoring sites glyoxal VCDs shown positive correlation with relative humidity and an anti-correlation factor was observed with temperature and solar irradiance. Particularly, significant correlation was found for glyoxal VCDs with solar irradiance over both sites (i,e, r = - 0.81 & r = - 0.82), while correlation with temperature (i,e, r = - 0.66 and r = - 0.52), and relative humidity were found a bit less significant (i,e, r = 0.51 & r = 0.63), as shown in Figure 4.1.4 (c)

A significant difference in temperature can be observed over both monitoring sites, but still June and July are among the hottest months of the year. This difference in temperature is primarily due to the difference in topography, geographic location and vegetation type that plays significant role as photosynthesis and temperature triggers the emissions of biogenic sources of glyoxal precursor (i,e, isoprene/monoterpene etc.) (Alvarado *et al.,* 2014; MacDonald *et al.*, 2012; Seinfeld & Pandis, 2012). Primarily, actinic flux and vegetation type/cover difference over Mainz and Islamabad caused the difference in diurnal concentration of glyoxal. However, temperature and relative humidity also contributed to some extent.

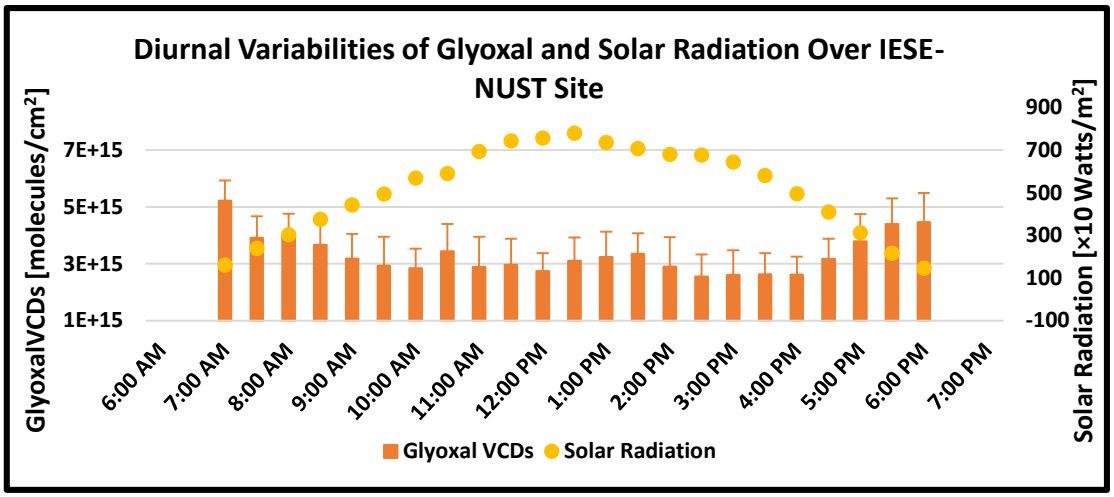

Figure 4.1.4 (a): Showing glyoxal diurnal variations in terms of VCDs (brown bars) over IESE, Pakistan. Glyoxal column densities and solar radiation (golden dots) were averaged over half an hour for the whole measurement time period.

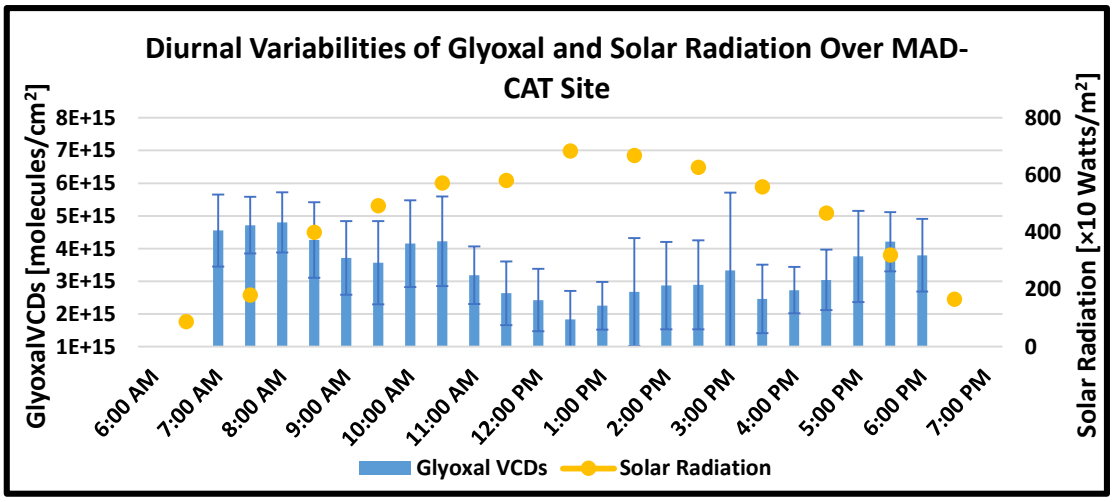

Figure 4.1.4 (b): Showing glyoxal diurnal variations in terms of VCDs (brown bars) over MPI-Ch, Germany. Glyoxal column densities and solar radiation (golden dots) were averaged over half an hour for the whole measurement time period.

Partially, anthropogenic emissions can be claimed for this observed difference in diurnal variations at both monitoring sites. Particularly in case of Pakistan; open burning of solid waste, vehicular exhaust (from vehicles not fitted with catalytic convertor) and use of low grade fuel in industries and for space heating purposes may cause enhanced glyoxal concentrations over Pakistan. In winters these anthropogenic contributions might be more clearly identified when ambient air temperature is very low and so the NMVOCs from biogenic emissions are minimal, at that time the observed glyoxal emission will be predominantly contributed from anthropogenic sources.

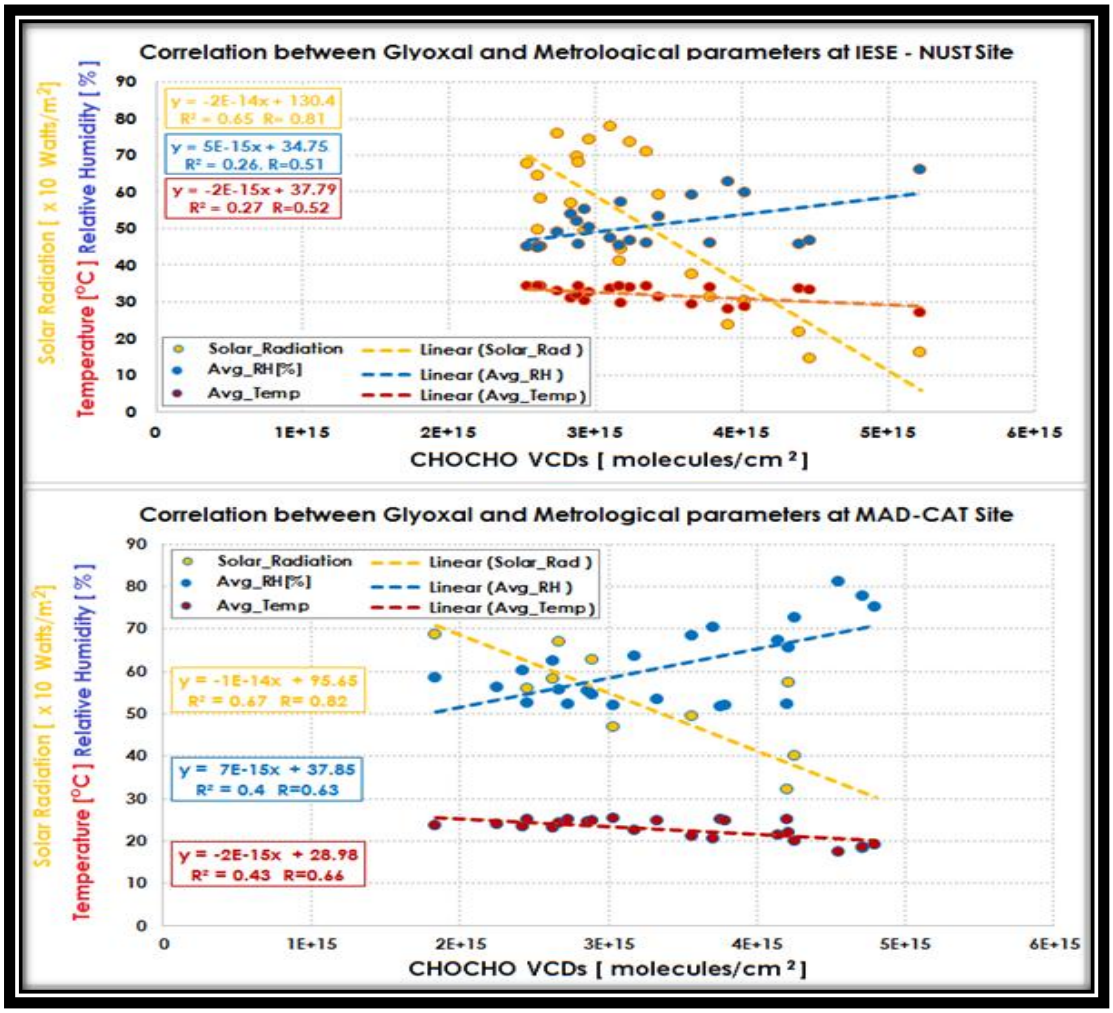

Figure 4.1.4 (c): Showing correlation plots between glyoxal daily mean VCDs and solar radiation (actinic flux - in golden), percentage relative humidity (in blue) and ambient air temperature (in red) over both of the monitoring sites at IESE, Islamabad (in upper panel) and at MPI-Ch, Mainz (in lower panel). In each scenario, respective correlation was calculated by applying linear fits.

4.2. Seasonal Cycle of Glyoxal Over Year (Oct-2014 to Sep-2015) at Site A

Glyoxal concentrations were observed to increase in the month of November and December and then gradually starts decreasing from January and the minimum concentration was detected for the month of April and it again starts rising from May and continued until the second seasonal peak was achieved in the month of August and after that it again started decreasing for September and October. A pictorial view of seasonal cycle is shown in fig. 4.2 (a) and time series of glyoxal for the monitoring time period is shown in fig 4.2 (b)

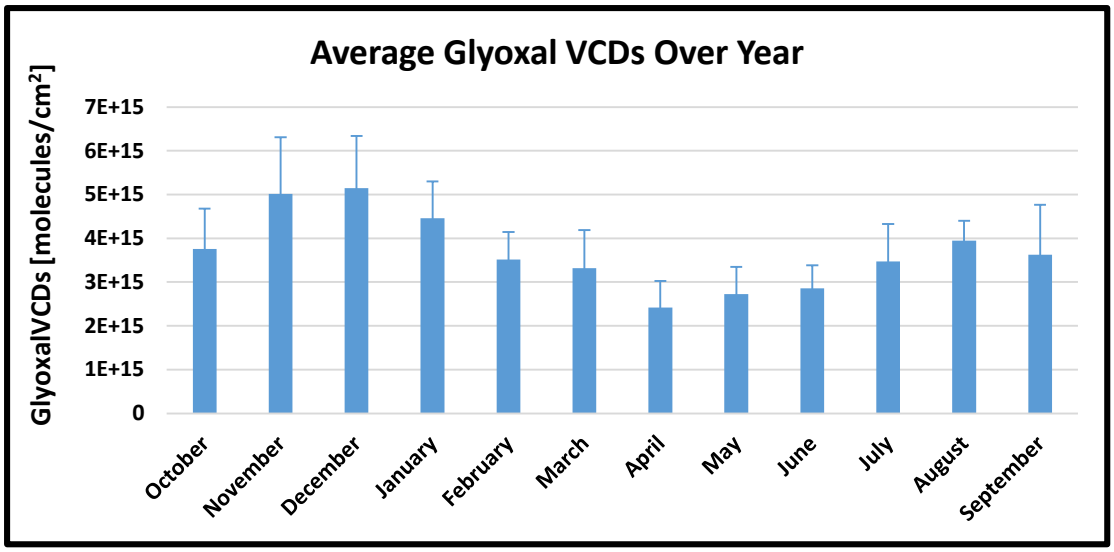

Figure: 4.2 (a): Seasonal cycle of glyoxal in terms of vertical column densities (molecules/cm^2) over year (Oct-2014 to Sep-2015)

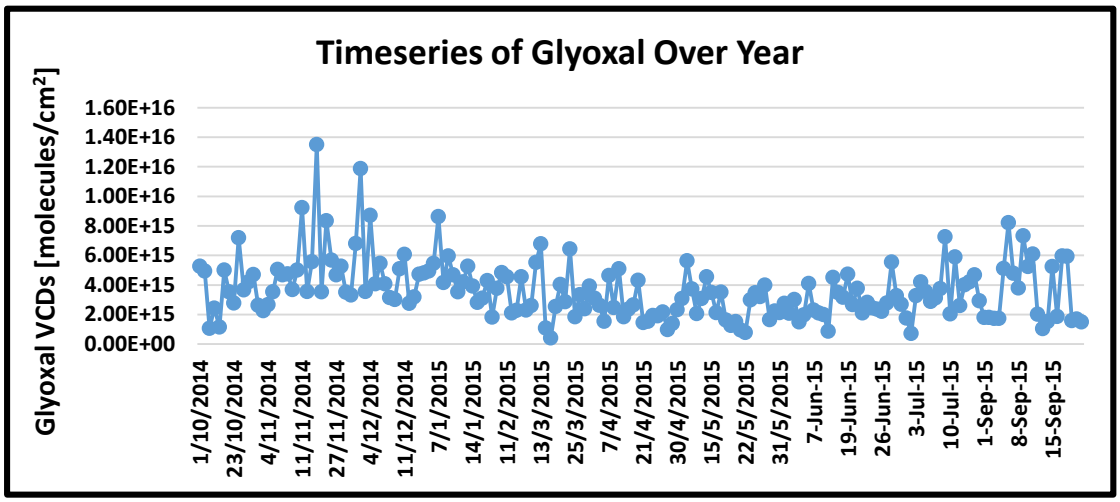

Figure: 4.2 (b): Time series of glyoxal in terms of vertical column densities (molecules/cm^2) measured over the monitoring period (Oct-2014 to Sep-2015)

4.3. Comparison of Seasonal Cycle with Metrological Parameters

Temperature and solar radiation profile showed anti-correlation with seasonal cycle of glyoxal. In the winter season primary source of glyoxal production is anthropogenic like open burning of solid waste, use of low grade fuel for domestic heating and also for commercial heating (Kleindienst *et al.*, 1986; McDonald *et al.*, 2000), and from traffic exhaust, especially from the vehicles, not fitted with catalytic convertors and exhaust filters. Production of photochemical smog from vehicular exhaust also gives rise to the formation of this compound as a secondary product of anthropogenic emissions (Jing *et al.*, 2001). Because of shorter day length in winters overhead Sun has low heat intensity and shiny hours, resulting in low biogenic glyoxal

production from isoprene, mainly terpenes and monoterpenes (Guenther *et al.*, 1995). And the collective glyoxal produced get less exposure to Sun light and the process of photolysis becomes slower resulting in high background concentration accumulation of glyoxal in the atmosphere.

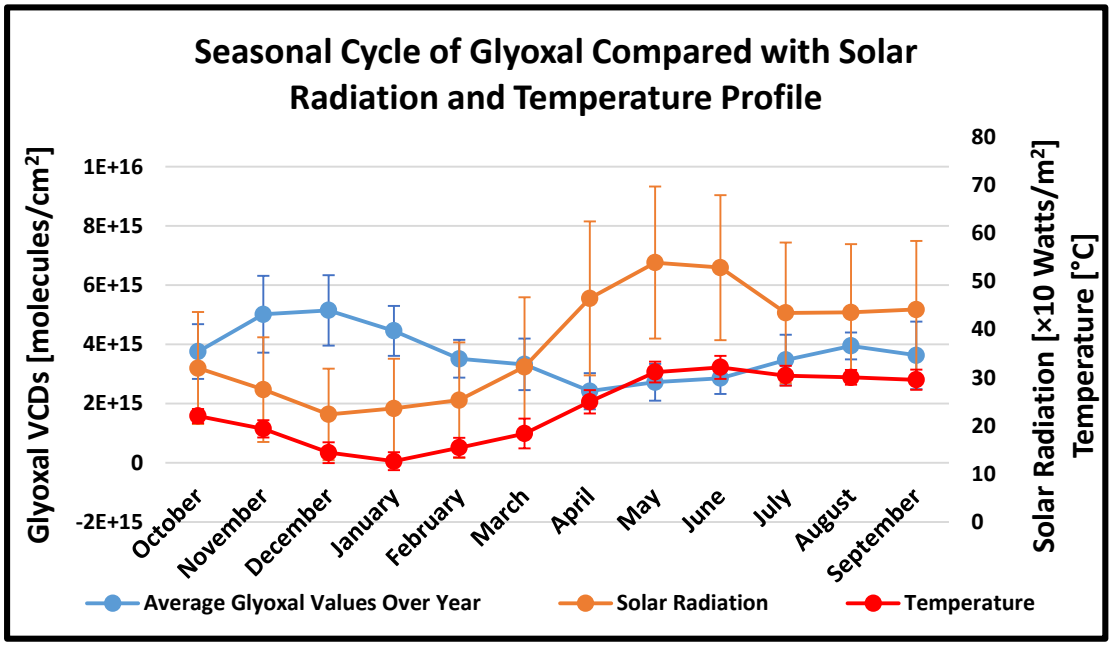

Figure: 4.3 (a): Seasonal cycle of glyoxal in terms of vertical column densities (molecules/cm^2: in blue) compared with solar radiation (Solar Radiation [×10 Watts/m^2]: in orange) and temperature (Temperature [°C]: in red) over year (Oct-2014 to Sep-2015).

In summer season net glyoxal production rate is higher than that of in winter as more biogenic production (Guenther *et al.*, 2000) due to brighter overhead Sun for longer days of the year and anthropogenic contributions. But in comparison to the production rate, detection rate of glyoxal is far lower in summers, as it is detectable throughout the day time but its concentration starts decreasing, due to OH photolysis, as the day proceeds and becomes minimum during noon and again starts rising near the evening due to lesser rate of photolysis (Volkamer *et al.*, 2005). In figure 4.3 (a) comparison of glyoxal seasonal cycle with temperature and solar radiation is shown.

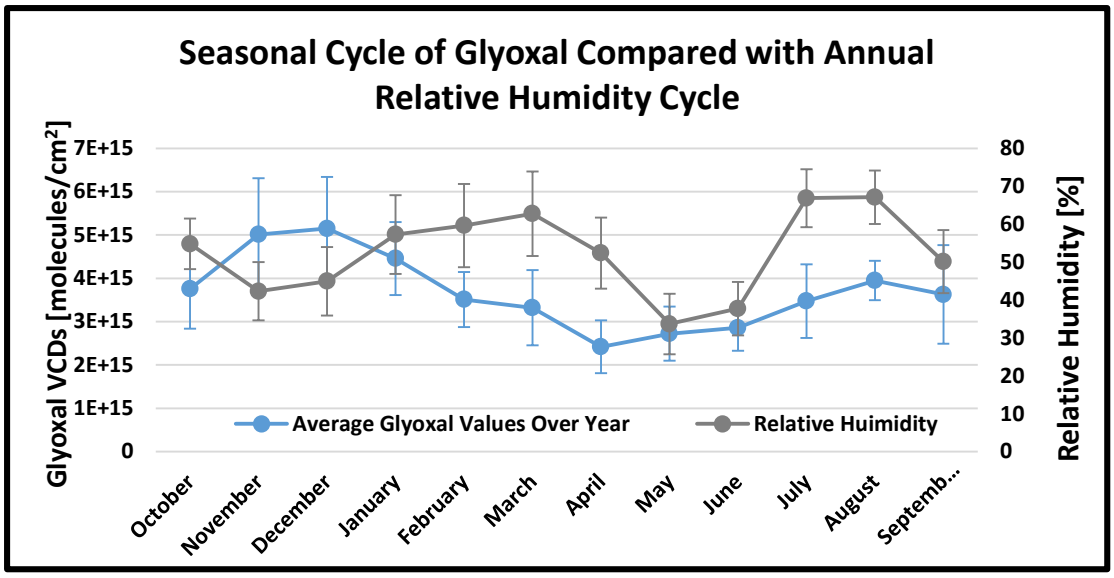

Figure: 4.3 (b): Seasonal cycle of glyoxal in terms of vertical column densities (molecules/cm^2: in blue) compared with relative humidity (Relative Humidity [%]: in grey) over year (Oct-2014 to Sep-2015).

In Figure 4.3 (b) seasonal cycle of glyoxal is compared with annual % relative humidity. Glyoxal column densities has shown positive correlation with relative humidity for entire seasonal cycle, over the year Oct-2014 to Sep-2015, except for the months of October, November and December. As the relative humidity is lowest in the months of May and June and so the retrieved glyoxal is.

CHAPTER 5

CONCLUSIONS AND RECOMMENDATIONS

4.1. Conclusions:

This is a pioneer work in Pakistan providing valuable information regarding glyoxal measurements from mini MAX-DOAS observations and comparison of the local data with an international field campaign. Glyoxal plays vital role in tropospheric air chemistry. As it is acts as a significant ring cleavage product in VOC photochemistry occurring in the terrestrial boundary layer (Volkamer *et al.*, 2005). Comparative results have shown a comparable trend in diurnal cycle of glyoxal column densities retrieved at both monitoring sites for the months of June and July for year 2013 and 2015 respectively. Actinic flux ($r > 0.8$) and vegetation profile has shown substantial impact on glyoxal emissions over both study sites when compared to relative humidity and temperature. Quantitative differences in glyoxal column densities are mainly due to the difference in solar irradiance (actinic flux), temperature and vegetation profile. Seasonal Cycle of measured glyoxal column densities, over Site A, has shown negative correlation with actinic flux and temperature, and positive correlation with relative humidity.

4.2. Recommendations:

1. Regular ambient air monitoring should be done for the generation of authentic National data base. And NEQS (national environmental quality standards) should be formulated.

2. In order to control traffic pollution, carpooling and mass transit system should be introduced in larger Urban areas of Pakistan.

3. In addition, public awareness should be done through effective media campaigns to improve the understanding and concern for air quality among public. And educating children at school level to develop a sense of responsibility to care our environment.

4. Air quality monitoring should be done at national, provincial as well as at city level.

5. Better understanding of the glyoxal production from oxidation of isoprene, terpenes and monoterpenes is also required.

6. In addition, data can be used as a reference by policy makers, environmental agencies, researchers, and non-governmental organizations (NGOs) working on different aspects of air pollution i.e. health impacts, climate change and for better mitigation and adaptation studies.

REFERENCES

REFERENCES

Ahmed, A. (2014). Pakistan's urban air pollution off the charts: World Bank.

Akimoto, H. (2016). Introduction to Atmospheric Chemistry *Atmospheric Reaction Chemistry* (pp. 1-9): Springer.

Alvarado, L., Richter, A., Vrekoussis, M., Wittrock, F., Hilboll, A., Schreier, S., & Burrows, J. (2014). An improved glyoxal retrieval from OMI measurements. *Atmos Meas Tech, 7*(12), 4133-4150.

Atkinson, R. (2000). Atmospheric chemistry of VOCs and NO x. *Atmospheric environment, 34*(12), 2063-2101.

Atkinson, R., Baulch, D., Cox, R., Crowley, J., Hampson, R., Hynes, R., . . . Subcommittee, I. (2006). Evaluated kinetic and photochemical data for atmospheric chemistry: Volume II–gas phase reactions of organic species. *Atmospheric Chemistry and Physics, 6*(11), 3625-4055.

Ban-Weiss, G. A., McLaughlin, J. P., Harley, R. A., Kean, A. J., Grosjean, E., & Grosjean, D. (2008). Carbonyl and nitrogen dioxide emissions from gasoline-and diesel-powered motor vehicles. *Environmental Science & Technology, 42*(11), 3944-3950.

Betterton, E. A., & Hoffmann, M. R. (1988). Henry's law constants of some environmentally important aldehydes. *Environmental Science & Technology, 22*(12), 1415-1418.

BLOEMEN, H. J. T. (1995). Chemistry and Analysis of Volatile Organic Compounds in the Environment

Bogumil, K., Orphal, J., Homann, T., Voigt, S., Spietz, P., Fleischmann, O., . . . Bovensmann, H. (2003). Measurements of molecular absorption spectra with the SCIAMACHY pre-flight model: instrument characterization and reference data for atmospheric remote-sensing in the 230–2380 nm region. *Journal of Photochemistry and Photobiology A: Chemistry, 157*(2), 167-184.

Bohn, B., & Zetzsch, C. (1998). Formation of HO 2 from OH and C 2 H 2 in the presence of O 2. *Journal of the Chemical Society, Faraday Transactions, 94*(9), 1203-1210.

Borrego, C., Gomes, P., Barros, N., & Miranda, A. (2000). Importance of handling organic atmospheric pollutants for assessing air quality. *Journal of Chromatography A, 889*(1), 271-279.

Calvert, J. G., Atkinson, R., Becker, K. H., Kamens, R. M., Seinfeld, J. H., Wallington, T. J., & Yarwood, G. (2002). *The mechanisms of atmospheric oxidation of aromatic hydrocarbons*: Oxford University Press New York.

Calvert, J. G., Atkinson, R., Kerr, J., Madronich, S., Moortgat, G., Wallington, T. J., & Yarwood, G. (2000). *The mechanisms of atmospheric oxidation of the alkenes* (Vol. 5): Oxford University Press New York.

Chebbi, A., & Carlier, P. (1996). Carboxylic acids in the troposphere, occurrence, sources, and sinks: A review. *Atmospheric environment, 30*(24), 4233-4249.

Christian, T. J., Kleiss, B., Yokelson, R. J., Holzinger, R., Crutzen, P., Hao, W. M., . . . Ward, D. E. (2003). Comprehensive laboratory measurements of biomass-burning emissions: 1. Emissions from Indonesian, African, and other fuels. *Journal of Geophysical Research: Atmospheres, 108*(D23).

Coburn, S., Dix, B., Sinreich, R., & Volkamer, R. (2011). The CU ground MAX-DOAS instrument: characterization of RMS noise limitations and first measurements near Pensacola, FL of BrO, IO, and CHOCHO. *Atmospheric Measurement Techniques, 4*(11), 2421-2439.

Danckaert, T., Fayt, C., Roozendale, M. V., Smedt, I. D., Letocart, V., Merlaud, A., & Pinardi, G. (2015). *QDOAS*

Software user manual. Belgian Institute for Space Aeronomy.

Fayt, C., & Van Roozendael, M. (2001). WinDOAS 2.1–Software user manual. *Uccle, belgium, bira-iasb*.

Fick, J., Nilsson, C., & Andersson, B. (2004). Formation of oxidation products in a ventilation system. *Atmospheric environment, 38*(35), 5895-5899.

Fick, J., Pommer, L., Nilsson, C., & Andersson, B. (2003). Effect of OH radicals, relative humidity, and time on the composition of the products formed in the ozonolysis of α-pinene. *Atmospheric environment, 37*(29), 4087-4096.

Finlayson-Pitts, B., & Pitts Jr, J. (2000). Chemistry of the Upper and Lower Atmosphere—Theory, Experiments, and Applications (Academic, San Diego).

Finlayson-Pitts, B. J., & Pitts Jr, J. N. (1999). *Chemistry of the upper and lower atmosphere: theory, experiments, and applications*: Academic press.

Frieß, U., Monks, P., Remedios, J., Rozanov, A., Sinreich, R., Wagner, T., & Platt, U. (2006). MAX-DOAS O4 measurements: A new technique to derive information on atmospheric aerosols: 2. Modeling studies. *Journal of Geophysical Research: Atmospheres, 111*(D14).

Fu, T. M., Jacob, D. J., Wittrock, F., Burrows, J. P., Vrekoussis, M., & Henze, D. K. (2008). Global budgets of atmospheric glyoxal and methylglyoxal, and implications for formation of secondary organic aerosols. *Journal of Geophysical Research: Atmospheres, 113*(D15).

Greenberg, J., Friedli, H., Guenther, A., Hanson, D., Harley, P., & Karl, T. (2006). Volatile organic emissions from the distillation and pyrolysis of vegetation. *Atmospheric Chemistry and Physics, 6*(1), 81-91.

Greenblatt, G. D., Orlando, J. J., Burkholder, J. B., & Ravishankara, A. (1990). Absorption measurements of oxygen between 330 and 1140 nm. *Journal of Geophysical Research: Atmospheres, 95*(D11), 18577-18582.

Gregg, J. W., Jones, C. G., & Dawson, T. E. (2003). Urbanization effects on tree growth in the vicinity of New York City. *Nature, 424*(6945), 183-187.

Grosjean, D., Grosjean, E., & Gertler, A. W. (2001). On-road emissions of carbonyls from light-duty and heavy-duty vehicles. *Environmental Science & Technology, 35*(1), 45-53.

Guenther, A., Geron, C., Pierce, T., Lamb, B., Harley, P., & Fall, R. (2000). Natural emissions of non-methane volatile organic compounds, carbon monoxide, and oxides of nitrogen from North America. *Atmospheric environment, 34*(12), 2205-2230.

Guenther, A., Hewitt, C. N., Erickson, D., Fall, R., Geron, C., Graedel, T., . . . McKay, W. (1995). A global model of natural volatile organic compound emissions. *Journal of Geophysical Research: Atmospheres, 100*(D5), 8873-8892.

Guenther, C. (2006). Estimates of global terrestrial isoprene emissions using MEGAN (Model of Emissions of Gases and Aerosols from Nature). *Atmospheric Chemistry and Physics, 6*.

Hays, M. D., Geron, C. D., Linna, K. J., Smith, N. D., & Schauer, J. J. (2002). Speciation of gas-phase and fine particle emissions from burning of foliar fuels. *Environmental Science & Technology*, *36*(11), 2281-2295.

Heckel, A., Richter, A., Tarsu, T., Wittrock, F., Hak, C., Pundt, I., . . . Burrows, J. (2005). MAX-DOAS measurements of formaldehyde in the Po-Valley. *Atmospheric Chemistry and Physics*, *5*(4), 909-918.

Hendrick, F., Roozendael, M. V., Kylling, A., Petritoli, A., Rozanov, A., Sanghavi, S., . . . Wittrock, F. (2006). Intercomparison exercise between different radiative transfer models used for the interpretation of ground-based zenith-sky and multi-axis DOAS observations. *Atmospheric Chemistry and Physics*, *6*(1), 93-108.

Hermans, C. Measurement of absorption cross sections and spectroscopic molecular parameters: O2 and its collisional induced absorption

Retrieved 29 feb 2015, 2002, from http://spectrolab.aeronomie.be/o2.htm

Ho, S. S. H., & Yu, J. Z. (2002). Concentrations of formaldehyde and other carbonyls in environments affected by incense burning. *Journal of Environmental Monitoring*, *4*(5), 728-733.

Hönninger, G., Friedeburg, C. v., & Platt, U. (2004). Multi axis differential optical absorption spectroscopy (MAX-DOAS). *Atmospheric Chemistry and Physics*, *4*(1), 231-254.

Huisman, A., Hottle, J., Galloway, M., DiGangi, J., Coens, K., Choi, W., . . . Gouw, J. d. (2011). Photochemical modeling of glyoxal at a rural site: observations and analysis from BEARPEX 2007. *Atmospheric Chemistry and Physics*, *11*(17), 8883-8897.

Jang, M., Czoschke, N. M., Lee, S., & Kamens, R. M. (2002). Heterogeneous atmospheric aerosol production by acid-catalyzed particle-phase reactions. *Science*, *298*(5594), 814-817.

Jang, M., & Kamens, R. M. (2001). Characterization of secondary aerosol from the photooxidation of toluene in the presence of NO x and 1-propene. *Environmental science & technology*, *35*(18), 3626-3639.

Jing, L., Steinberg, S. M., & Johnson, B. J. (2001). Aldehyde and monocyclic aromatic hydrocarbon mixing ratios at an urban site in Las Vegas, Nevada. *Journal of the air & waste management association*, *51*(9), 1359-1366.

Kanakidou, M., Seinfeld, J., Pandis, S., Barnes, I., Dentener, F., Facchini, M., . . . Nielsen, C. (2005). Organic aerosol and global climate modelling: a review. *Atmospheric Chemistry and Physics, 5*(4), 1053-1123.

Kean, A. J., Grosjean, E., Grosjean, D., & Harley, R. A. (2001). On-road measurement of carbonyls in California light-duty vehicle emissions. *Environmental Science & Technology, 35*(21), 4198-4204.

Kielhorn, J., Pohlenz-Michel, C., Schmidt, S., & Mangelsdorf, I. (2004). Concise International Chemical Assessment Document 57, Glyoxal. *World Health Organization*.

Kleindienst, T. E., Shepson, P. B., Edney, E. O., Claxton, L. D., & Cupitt, L. T. (1986). Wood smoke: measurement of the mutagenic activities of its gas-and particulate-phase photooxidation products. *Environmental science & technology, 20*(5), 493-501.

Kraus, D. (2006). *A Framework Design for DOAS.* PhD-thesis, University of Mannheim (h ttp://hci. iwr. uni-heidelberg. de/publications/dip/2006/Kraus PhD2006. pdf).

Kurucz, R. L., Furenlid, I., Brault, J., & Testerman, L. (1984). Solar Flux Atlas from 296 to 1300 nm. *National Solar Observatory Atlas, Sunspot, New Mexico: National Solar Observatory, 1984, 1*.

Lamb, B., Guenther, A., Gay, D., & Westberg, H. (1987). A national inventory of biogenic hydrocarbon emissions. *Atmospheric Environment (1967), 21*(8), 1695-1705.

Lee, Y., Zhou, X., Kleinman, L., Nunnermacker, L., Springston, S., Daum, P., . . . Spicer, C. (1998). Atmospheric chemistry and distribution of formaldehyde and several multioxygenated carbonyl compounds during the 1995 Nashville/Middle Tennessee Ozone Study. *Journal of Geophysical Research, 103*(D17), 22449-22462.

Leser, H., Hönninger, G., & Platt, U. (2003). MAX-DOAS measurements of BrO and NO2 in the marine boundary layer. *Geophysical Research Letters, 30*(10).

Li, X., Brauers, T., Hofzumahaus, A., Lu, K., Li, Y., Shao, M., . . . Wahner, A. (2013). MAX-DOAS measurements of NO 2, HCHO and CHOCHO at a rural site in Southern China. *Atmospheric Chemistry and Physics, 13*(4), 2133-2151.

Liggio, J., Li, S.-M., & McLaren, R. (2005). Heterogeneous reactions of glyoxal on particulate matter: Identification of acetals and sulfate esters. *Environmental science & technology, 39*(6), 1532-1541.

Lopez, A., Ricco, G., Ciannarella, R., Rozzi, A., Di Pinto, A., & Passino, R. (1999). Textile wastewater reuse: ozonation of membrane concentrated secondary effluent. *Water science and technology, 40*(4), 99-105.

MacDonald, S., Oetjen, H., Mahajan, A., Whalley, L., Edwards, P., Heard, D., . . . Plane, J. (2012). DOAS measurements of formaldehyde and glyoxal above a south-east Asian tropical rainforest. *Atmospheric Chemistry and Physics, 12*(13), 5949-5962.

McDonald, J. D., Zielinska, B., Fujita, E. M., Sagebiel, J. C., Chow, J. C., & Watson, J. G. (2000). Fine particle and gaseous emission rates from residential wood combustion. *Environmental science & technology, 34*(11), 2080-2091.

Mo, W., & Li, M. (1992). Effects of Cd2+ on the cell division of root tip in bean seedlings. *Bulletin of Botany, 9*(3), 30-34.

Molina, L. T., & Molina, M. J. (2002). *Air quality in the Mexico megacity: an integrated assessment* (Vol. 15): SciELO Chile.

Mopper, K., & Stahovec, W. L. (1986). Sources and sinks of low molecular weight organic carbonyl compounds in seawater. *Marine Chemistry, 19*(4), 305-321.

Moree-Testa, P., & Saint-Jalm, Y. (1981). Determination of α-dicarbonyl compounds in cigarette smoke. *Journal of Chromatography A, 217*, 197-208.

Munger, J. W., Jacob, D. J., Daube, B. C., Horowitz, L., Keene, W., & Heikes, B. (1995). Formaldehyde, glyoxal, and methylglyoxal in air and cloudwater at a rural mountain site in central Virginia.

Myriokefalitakis, S., Vrekoussis, M., Tsigaridis, K., Wittrock, F., Richter, A., Brühl, C., . . . Kanakidou, M. (2008). The influence of natural and anthropogenic secondary sources on the glyoxal global distribution. *Atmospheric Chemistry and Physics, 8*(16), 4965-4981.

Nunes, F. M. N., Veloso, M., Pereira, P. d. P., & De Andrade, J. (2005). Gas-phase ozonolysis of the monoterpenoids (S)-(+)-carvone,(R)-(−)-carvone,(−)-carveol, geraniol and citral. *Atmospheric environment, 39*(40), 7715-7730.

Partridge, P. A., Shala, F. J., Cernansky, N. P., & Suffet, I. H. (1987). Characterization and analysis of diesel exhaust odor. *Environmental Science & Technology, 21*(4), 403-408.

Pikelnaya, O., Hurlock, S. C., Trick, S., & Stutz, J. (2007). Intercomparison of multiaxis and long-path differential optical absorption spectroscopy measurements in the marine boundary layer. *Journal of Geophysical Research: Atmospheres, 112*(D10).

Pitts, B. F., & Pitts, J. (2000). Chemistry of the upper and lower atmosphere: Theory, experiments and applications. *Academic, US*.

Pitts, J., Atkinson, R., Winer, A., Arey, J., & Tuazon, E. (1985). Formation and fate of toxic chemicals in California's atmosphere. Final report, July 10, 1984-November 22, 1985: California Univ., Riverside (USA). Statewide Air Pollution Research Center.

Platt, U., & Stutz, J. (2008). *Differential absorption spectroscopy*: Springer.

Pope III, C. A., & Dockery, D. W. (2006). Health effects of fine particulate air pollution: lines that connect. *Journal of the air & waste management association, 56*(6), 709-742.

Possanzini, M., Tagliacozzo, G., & Cecinato, A. (2007). Ambient levels and sources of lower carbonyls at Montelibretti, Rome (Italy). *Water, air, and soil pollution, 183*(1-4), 447-454.

Ramanathan, V., Callis, L., Cess, R., Hansen, J., Isaksen, I., Kuhn, W., . . . Reck, R. (1987). Climate-chemical interactions and effects of changing atmospheric trace gases. *Reviews of Geophysics, 25*(7), 1441-1482.

Ramanathan, V., & Crutzen, P. (2003). New directions: Atmospheric brown "clouds". *Atmospheric environment, 37*(28), 4033-4035.

Ramanathan, V., Crutzen, P., Kiehl, J., & Rosenfeld, D. (2001). Aerosols, climate, and the hydrological cycle. *Science, 294*(5549), 2119-2124.

Roberts, G. C., Artaxo, P., Zhou, J., Swietlicki, E., & Andreae, M. O. (2002). Sensitivity of CCN spectra on chemical and physical properties of aerosol: A case study from the Amazon Basin. *Journal of Geophysical Research: Atmospheres, 107*(D20).

Rothman, L. S. (2010). The evolution and impact of the HITRAN molecular spectroscopic database. *Journal of Quantitative Spectroscopy and Radiative Transfer, 111*(11), 1565-1567.

Rothman, L. S., Jacquemart, D., Barbe, A., Benner, D. C., Birk, M., Brown, L., . . . et al. (2005). The HITRAN 2004 molecular spectroscopic database. *Journal of Quantitative Spectroscopy and Radiative Transfer, 96*(2), 139-204.

Seinfeld, J. H., & Pandis, S. N. (2012). *Atmospheric chemistry and physics: from air pollution to climate change*: John Wiley & Sons.

Setokuchi, O. (2011). Trajectory calculations of OH radical-and Cl atom-initiated reaction of glyoxal: atmospheric chemistry of the HC (O) CO radical. *Physical Chemistry Chemical Physics, 13*(13), 6296-6304.

Sinreich, R., Volkamer, R., Filsinger, F., Frieß, U., Kern, C., Platt, U., . . . Wagner, T. (2007). MAX-DOAS detection of glyoxal during ICARTT 2004. *Atmospheric Chemistry and Physics, 7*(5), 1293-1303.

Spaulding, R. S., Schade, G. W., Goldstein, A. H., & Charles, M. J. (2003). Characterization of secondary atmospheric photooxidation products: Evidence for biogenic and anthropogenic sources. *Journal of Geophysical Research: Atmospheres, 108*(D8).

Stavrakou, T., Müller, J.-F., Smedt, I. D., Roozendael, M. V., Kanakidou, M., Vrekoussis, M., . . . Burrows, J. (2009). The continental source of glyoxal estimated by the synergistic use of spaceborne measurements and inverse modelling. *Atmospheric Chemistry and Physics, 9*(21), 8431-8446.

Tadić, J., Moortgat, G. K., & Wirtz, K. (2006). Photolysis of glyoxal in air. *Journal of Photochemistry and Photobiology A: Chemistry, 177*(2), 116-124.

Thalman, R., & Volkamer, R. (2013). Temperature dependent absorption cross-sections of O 2–O 2 collision pairs between 340 and 630 nm and at atmospherically relevant pressure. *Physical Chemistry Chemical Physics, 15*(37), 15371-15381.

Tsigaridis, K., & Kanakidou, M. (2003). Global modelling of secondary organic aerosol in the troposphere: a sensitivity analysis. *Atmospheric Chemistry and Physics, 3*(5), 1849-1869.

Tsigaridis, K., & Kanakidou, M. (2007). Secondary organic aerosol importance in the future atmosphere. *Atmospheric environment, 41*(22), 4682-4692.

Tsigaridis, K., Lathiere, J., Kanakidou, M., & Hauglustaine, D. (2005). Naturally driven variability in the global secondary organic aerosol over a decade. *Atmospheric Chemistry and Physics, 5*(7), 1891-1904.

Van Roozendael, M., Fayt, C., Post, P., Hermans, C., & Lambert, J. (2003). Retrieval of BrO and NO2 from UV-visible observations. *Sounding the troposphere from space: a new era for atmospheric chemistry, Springer-Verlag, ISBN*, 3-540.

Vandaele, A. C., Hermans, C., Simon, P. C., Carleer, M., Colin, R., Fally, S., . . . Coquart, B. (1998). Measurements of the NO 2 absorption cross-section from 42 000 cm− 1 to 10 000 cm− 1 (238–1000 nm) at 220 K and 294 K. *Journal of Quantitative Spectroscopy and Radiative Transfer, 59*(3), 171-184.

Voigt, S., Orphal, J., Bogumil, K., & Burrows, J. (2001). The temperature dependence (203–293 K) of the absorption cross sections of O 3 in the 230–850 nm region measured by Fourier-transform spectroscopy. *Journal of Photochemistry and Photobiology A: Chemistry, 143*(1), 1-9.

Voigt, S., Orphal, J., & Burrows, J. (2002). The temperature and pressure dependence of the absorption cross-sections of NO 2 in the 250–800 nm region measured by Fourier-transform spectroscopy. *Journal of Photochemistry and Photobiology A: Chemistry, 149*(1), 1-7.

Volkamer, R., Jimenez, J. L., San Martini, F., Dzepina, K., Zhang, Q., Salcedo, D., . . . Molina, M. J. (2006). Secondary organic aerosol formation from anthropogenic air pollution: Rapid and higher than expected. *Geophysical Research Letters, 33*(17).

Volkamer, R., Molina, L. T., Molina, M. J., Shirley, T., & Brune, W. H. (2005). DOAS measurement of glyoxal as an indicator for fast VOC chemistry in urban air. *Geophysical Research Letters, 32*(8).

Volkamer, R., Platt, U., & Wirtz, K. (2001). Primary and secondary glyoxal formation from aromatics: Experimental evidence for the bicycloalkyl-radical pathway from benzene, toluene, and p-xylene. *The Journal of Physical Chemistry A, 105*(33), 7865-7874.

Volkamer, R., San Martini, F., Molina, L. T., Salcedo, D., Jimenez, J. L., & Molina, M. J. (2007). A missing sink for gas-phase glyoxal in Mexico City: Formation of secondary organic aerosol. *Geophysical Research Letters, 34*(19).

Volkamer, R., Spietz, P., Burrows, J., & Platt, U. (2005). High-resolution absorption cross-section of glyoxal in the UV–vis and IR spectral ranges. *Journal of Photochemistry and Photobiology A: Chemistry, 172*(1), 35-46.

Vrekoussis, M., Wittrock, F., Richter, A., & Burrows, J. (2009). Temporal and spatial variability of glyoxal as observed from space. *Atmospheric Chemistry and Physics, 9*(13), 4485-4504.

Wagner, T., Burrows, J., Deutschmann, T., Dix, B., Friedeburg, C. v., Frieß, U., . . . Iwabuchi, H. (2007). Comparison of box-air-mass-factors and radiances for Multiple-Axis Differential Optical Absorption Spectroscopy (MAX-DOAS) geometries calculated from different UV/visible radiative transfer models. *Atmospheric Chemistry and Physics, 7*(7), 1809-1833.

Wayne, R. (2000). Chemistry of Atmospheres, 3rd: Oxford University Press, Inc.: New York, USA.

Wittrock, F., Oetjen, H., Richter, A., Fietkau, S., Medeke, T., Rozanov, A., & Burrows, J. (2004). MAX-DOAS measurements of atmospheric trace gases in Ny-Ålesund-Radiative transfer studies and their application. *Atmospheric Chemistry and Physics, 4*(4), 955-966.

Xiao, Y., Jacob, D. J., & Turquety, S. (2007). Atmospheric acetylene and its relationship with CO as an indicator of air mass age. *Journal of Geophysical Research: Atmospheres, 112*(D12).

Yu, S. (2000). Role of organic acids (formic, acetic, pyruvic and oxalic) in the formation of cloud condensation nuclei (CCN): a review. *Atmospheric Research, 53*(4), 185-217.

Zhou, X., & Mopper, K. (1990). Measurement of sub-parts-per-billion levels of carbonyl compounds in marine air by a simple cartridge trapping procedure followed by liquid chromatography. *Environmental Science & Technology, 24*(10), 1482-1485.